EUROPEAN ORGANIZATION FOR NUCLEAR RESEARCH

CERN-SPSC-2005-030
SPSC-P-327
16 June 2006

ELECTROMAGNETIC PROCESSES IN STRONG CRYSTALLINE FIELDS

J.U. Andersen, K. Kirsebom, S.P. Møller, A.H. Sørensen, U.I. Uggerhøj
Department of Physics and Astronomy, Aarhus University, Denmark

A. Apyan
Department of Physics and Astronomy, Northwestern University, Evanston IL, USA

P. Sona
Institute of Physics, Florence University, Italy

S. Ballestrero, S. Connell
Schonland Research Institute, Johannesburg, South Africa

T. Ketel
Science Department, Free University, Amsterdam, The Netherlands

M. Khokonov
Department of Physics, Kabardino-Balkarian State University, Nalchik, Russian Fed.

V. Biryukov, Yu. Chesnokov
Institute of High Energy Physics, Protvino, Russia

W. Greiner, A.V. Korol, A.V. Solov'yov
Frankfurt Institute for Advanced Studies, Johann Wolfgang Goethe University, Frankfurt, Germany

V. Baier
Budker Institute of Nuclear Physics, Novosibirsk, Russia

S. Kartal, A. Dizdar
Department of Physics, University of Istanbul, Turkey

A. Mangiarotti
Universidada de Coimbra, Coimbra, Portugal

Yu. Kononets
Kurchatov Institute, Moscow, Russia

Abstract

We propose a number of new investigations on aspects of radiation from high energy electron and positron beams (10-300 GeV) in single crystals and amorphous targets. The common heading is radiation emission by electrons and positrons in strong electromagnetic fields, but as the setup is quite versatile, other related phenomena in radiation emission can be studied as well. The intent is to clarify the role of a number of important aspects of radiation in strong fields as e.g. observed in crystals. We propose to measure trident 'Klein-like' production in strong crystalline fields, 'crystalline undulator' radiation, 'sandwich' target phenomena, LPM suppression of pair production as well as axial and planar effects in contributions of spin to the radiation.

Contents

1 Introduction

In the 1990's, the NA43 collaboration [1] investigated a number of phenomena in strong field QED among which can be mentioned: radiation emission in crystals [2], pair production [3], shower formation [4], axial radiative cooling [5] and the influence of spin on the radiation [6]. The knowledge gained on radiation processes by this collaboration has stimulated substantial activity in theoretical [7, 8, 9, 10, 11] as well as in related experimental areas that now render it very desirable to extend the measurements and pursue new phenomena. For a recent review of strong field effects in crystals, see [12].

Under small angles of incidence to a crystallographic direction - an axis or a plane - the strong electric fields of the nuclear constituents add coherently such as to obtain a macroscopic, continuous field with a peak value of the order $\mathcal{E} \simeq 10^{11}$ V/cm. Therefore, in the restframe of an ultrarelativistic electron with a Lorentz factor of $\gamma \simeq 10^5$, the field encountered becomes comparable to the critical (or Schwinger-) field, $\mathcal{E}_0 = m^2c^3/e\hbar = 1.32 \cdot 10^{16}$ V/cm, corresponding to a magnetic field $B_0 = 4.41 \cdot 10^9$ T. The incident particle moves in these immensely strong fields over distances up to that of the crystal thickness, i.e. up to several mm.

Since the quantity

$$\chi = \gamma\mathcal{E}/\mathcal{E}_0 \tag{1}$$

is a relativistic invariant for the transverse field $\mathcal{E}$, the behaviour of charged particles in fields as strong as $\mathcal{E}_0$ can be investigated by use of ultrarelativistic electrons in strong crystalline fields. Already at $\chi \simeq 0.1$ the synchrotron-like radiation emission attains a non-classical character [6]. An introduction to these 'strong field effects' can be found in [13, 12].

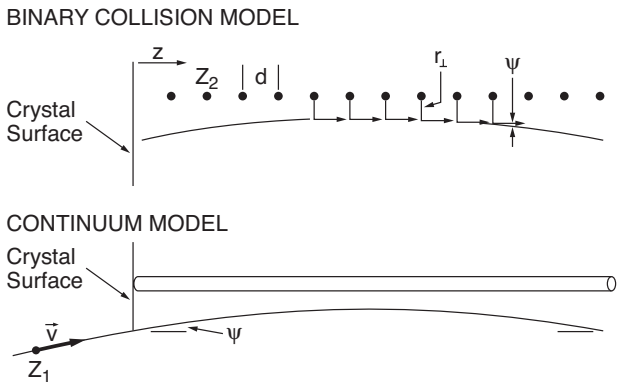

Figure 1: *A schematic drawing of the discrete atomic scattering centers in a crystal and the continuum approximation. The target atoms with atomic number Z_2 and distance d along the string, impose a curved trajectory on the penetrating particle with atomic number Z_1 through binary encounters over the transverse distance $r_\perp$. The resulting trajectory with entrance angle ψ can be accurately described as the result of interaction with a string of continuous charge distribution, corresponding to a 'smearing' of the charges Z_2e along the direction z of the rows of atoms.*

In CERNs NA48 experiment two applications of strong crystalline fields have been used: An efficient conversion of photons into electron-positron pairs to delimit the fiducial region [14] and a bent crystal to deflect a well-defined fraction of the main beam to generate kaons [15]. The first of these effects relies on the field in the rest-frame of an electron to be comparable to the magnitude of the Schwinger field. The second effect is due to deflection by the electric field from a plane of crystal atoms which is equivalent to a magnetic field of up to a few thousand Tesla in the bent crystal. Clearly, the fields attained are exceedingly high and offer new possibilities in fundamental physics as well as applications.

The proposed measurements will significantly enhance the understanding of QED processes in crystals and amorphous matter under special conditions, while also yielding insight into processes of astrophysical and practical importance, e.g. beamstrahlung, creation of QCD jets or radiation from highly magnetized neutron stars.

Our group has remained active at the CERN SPS during recent years, with various experiments in crystalline and radition emission phenomena, based on test beams in H2 and H4 [16, 17, 18, 19, 20, 21, 22, 23].

2 Strong crystalline fields

Three dimensionless invariants χ, Ξ, Γ can be constructed from the the electromagnetic field strength tensor, $F_{\mu\nu}$, and the momentum four-vector p^ν (or, in the case of a photon, $\hbar k^\nu$). For an ultra-relativistic particle moving across fields $\mathcal{E} \ll \mathcal{E}_0, B \ll B_0$ with an angle $\theta \gg 1/\gamma$ the invariants fulfill $\chi \gg \Xi, \Gamma$ and $\Xi, \Gamma \ll 1$. The relation of χ to the fields $\vec{\mathcal{E}}$ and $\vec{B}$ is given by [24]

$$\chi^2 = \frac{1}{\mathcal{E}_0^2 m^2 c^4}((\vec{p}c \times \vec{B} + E \cdot \vec{\mathcal{E}})^2 - (\vec{p}c \cdot \vec{\mathcal{E}})^2) \tag{2}$$

For an ultrarelativistic particle moving perpendicularly to a purely electric or purely magnetic field this reduces to

$$\chi = \frac{\gamma \mathcal{E}}{\mathcal{E}_0} \text{ or } \chi = \frac{\gamma B}{B_0} \tag{3}$$

which is identical to eq. (1).

For the emission of radiation it is the trajectory that is decisive. Therefore, it is insignificant if the field responsible for the path is electric or magnetic, and electric fields present in crystals may be used to investigate e.g. synchrotron radiation.

Since χ is invariant, γB (or $\gamma \mathcal{E}$) is the same in any reference system and thus it is reasonable to transform to the electron frame. In this reference system by definition the Lorentz factor of the electron is 1 and the field present in the frame of the laboratory is boosted by $\gamma = E/mc^2$, where E is the energy of the electron in the laboratory. This means that the field in the rest-frame of the electron can become critical for achievable γ-values.

2.1 Critical angles

For high energy particles penetrating single crystals, there are two angles of relevance for directional effects: The channeling (Lindhard) angle and the strong field (Baier) angle.

2.1.1 Channeling critical angles

When the particle approaches the center of the continuum string it has a fair chance - partly due to thermal vibrations - of acquiring a transverse energy exceeding the height of the transverse potential given by the smeared nuclear fields. So for an incident angle ψ_c to the axis where

$$E_\perp = \frac{1}{2} pv\psi_c^2 \simeq U(\rho_t) \tag{4}$$

where ρ_t is a thermal vibration amplitude, the particle may escape the well, i.e. be dechanneled. Using the Lindhard 'standard' potential [25], this gives for the axial effect a critical angle for channeling

$$\psi_1 = \sqrt{\frac{4Z_1 Z_2 e^2}{pvd}} \tag{5}$$

For the planar motion the critical angle is

$$\psi_p = \sqrt{\frac{4Z_1 Z_2 e^2 n d_p C_L a_s}{pv}} \tag{6}$$

and generally $\psi_1 \simeq 3\psi_p$ since the transverse axial and planar potentials differ by about a factor 10. Here, d_p denotes the planar distance, d the spacing of atoms along the axial direction, $Z_1 e$ is the charge of the penetrating particle, $C_L \simeq \sqrt{3}$ is Lindhard's constant and a_s is the (Thomas-Fermi) screening distance. The continuum picture does not become invalid beyond the critical angle but may persist out to angles as large as $50\psi_1$.

2.1.2 Characteristic angle for strong fields

Following [26], conservation of transverse energy leads to

$$\frac{p^2}{2\gamma m}\psi_0^2 = \frac{p^2}{2\gamma m}(\psi_0 + \Delta\psi)^2 - U_0 \tag{7}$$

where ψ_0 and $\Delta\psi$ denote the incident and deflection angle, respectively. For $\Delta\psi \ll \psi_0$ this gives

$$\Delta\psi = \frac{1}{\gamma}\frac{U_0}{mc^2}\frac{1}{\psi_0} \tag{8}$$

such that the angle

$$\Theta_0 = \frac{U_0}{mc^2} \tag{9}$$

separates two regions where the deflection angle is larger than or smaller than the opening angle of the emission cone, $1/\gamma$. Thus it separates the regions where the radiation has dipole nature, $\psi \gg \Theta_0$, and where it has a synchrotron nature, $\psi \ll \Theta_0$. Θ_0 is the so-called Baier-angle. This characteristic angle does not depend on energy such that at relatively high energies, roughly when $\gamma \simeq 2mc^2/U_0$, i.e. a few GeV for axes in Si and Ge, we have $\psi_c < \Theta_0$ since $\psi_c \propto 1/\sqrt{\gamma}$. Thus the strong field regime extends beyond the channeling regime for particles with energy above a few GeV. Furthermore, in accordance with the continuum approximation the field registered by a particle incident at this angle can be considered constant along the string.

At TeV energies - relevant for secondary particles in e.g. the lead tungstate single crystal calorimeters of ALICE - the relevant angles for directional effects are not the channeling angles, but the Baier angles which are a thousand times larger, in the mrad range.

3 Non-crystalline strong fields

3.1 Astrophysical strong fields

Following a semi-classical argument [27] we can calculate the excitation energy of an electron in a strong magnetic field, B_0. From the gyration radius $r_c = p_\perp c/eB$ and the uncertainty relation $r_c p \simeq \hbar$ we get a semi-classical gyration radius $r_c = \lambda_c\sqrt{B_0/B}$ and from $\omega \simeq c/r_c$ we finally get the relative excitation energy in a strong field

$$\frac{\hbar\omega}{mc^2} \simeq \sqrt{\frac{B}{B_0}} \tag{10}$$

which shows that the gyration becomes relativistic in fields $B \gtrsim B_0$. There is substantial evidence that pulsars with fields at and above this strength - so-called magnetars - exist. A recent example is the $\simeq 10^{11}$ T magnetar detected in the soft gamma repeater SGR 1806-20 [28] which yielded a giant flare at the end of 2004 [29].

3.2 Strong fields in nuclear collisions

As a measure of the electric field a $1s$ electron is exposed to, let us consider the ratio of this field to the critical field: $\mathcal{E}_{1s}/\mathcal{E}_0 = \alpha^3 Z^3$ where effects such as relativistic corrections, reduced mass and extension of the nucleus are neglected. Clearly, for a nuclear charge number of $Z = 137$ a $1s$ electron is in a strong field. Equivalently, the binding energy 'dives' into the negative energy continuum for $Z = 137$ (and for extended nuclei $Z \simeq 172$) and a pair is created. During the collision of two nuclei with a combined charge exceeding $172|e|$, a quasimolecular state with a very short existence may be generated from which e.g. positron emission has been observed. So by means of collisions of heavy nuclei, strong field QED may be investigated. However, since the nuclear collision is of extremely short duration, $\approx 10^{-22}$s, the strong field in this case is far from constant. For a review see e.g. [30].

3.3 Strong laser fields

Another technically demanding example of investigations of strong fields is in multi-GeV electron collisions with terawatt laser pulses where non-linear Compton scattering and so-called Breit-Wheeler

pair production are observed [31, 32]. Breit-Wheeler pair production is the production of an electron-positron pair in a photon-photon collision. In order to get sufficient energy in the center-of-mass system to pair produce, at least one of the photons must be very energetic. This has been achieved by non-linear Compton backscattering of laser photons off an intense, high-energy electron beam. In non-linear Compton backscattering, several photons are absorbed but only one is emitted. In this case again χ is a crucial parameter. For a future $\gamma\gamma$-collider, these strong field effects must be carefully avoided in order not to deplete the photon beams to be produced by Compton backscattering off intense laser pulses [33]. Moreover, the effect of the electron spin becomes even stronger in the case of interactions with strong laser fields as compared to crystalline strong field effects [34, 35].

Other theoretical schemes proposed to achieve fields approaching the Schwinger limit is by laser reflection off a relativistic 'mirror' made by a propagating wakefield in a plasma [36].

3.4 Strong fields in beam-beam interactions

In the construction of the next generation of linear colliders an important phenomenon is the emission of beamstrahlung due to the interaction of one bunch with the electromagnetic field from the opposing bunch. In the restframe of one bunch the field of the other bunch is boosted by a factor $2\gamma^2$ and may approach or even exceed critical field values. The emission of beamstrahlung can be expressed as a function of χ (often called Υ in the accelerator physics community) which for the Stanford Linear Collider (SLC) is small $\simeq 10^{-3}$ but of the order unity for the next generation linear colliders [37]. Thus for these future colliders $\gamma\gamma$-collisions may be generated from the beams themselves or special bunch structures must be applied to avoid rapid beam deterioration from strong field effects [38].

For a future linear collider operating in the 'quantum regime', the beamstrahlung spectrum becomes similar to the spectrum from multi-hundred GeV electrons passing single crystals, as shown below in fig. 12, to be compared to the full-drawn line in fig. 13.

3.5 The geomagnetic field as a strong field

With facilities like the Pierre Auger Observatory [39] for the detection of ultra high energy cosmic rays of energies in the EeV (10^{18} eV) region and orders of magnitude above, pair production and photon emission in the magnetic field of the Earth become increasingly relevant. This phenomenon has been studied first by [40], later revived by [41] and recently by e.g. [42] as well as in extended air shower simulations [43]. One important issue in this context is the possibility of distinguishing photon-initiated extended air showers from those initiated by protons or heavy nuclei. Such a distinction may shed light on the question of 'top-down' (topological defects, massive X-particles) or 'bottom-up' (acceleration of known particles) mechanisms [44, 45].

The behaviour of an EeV electromagnetic shower initiated in the Earth magnetic field and that of a GeV shower in a crystal are intimately related. This is so because the decisive χ is about equal in the two cases and their developments are both affected by e.g. multiple scattering and LPM effect [46]. The close analogy between the two processes makes crystals a suitable testing ground for the development of computer codes to simulate the behavior of extended air showers.

Finally, for sufficiently energetic photons even the intergalactic fields will appear as a strong field and generally speaking the Universe thus will become 'opaque' to these photons. As intergalactic fields are quite weak, $\approx 10^{-12}$ T, this happens at very high energies only.

In the following, we discuss each of the sub-experiments in view of their relevance and recent activities, theoretical as well as experimental.

4 Klein-like trident production

4.1 Theory

Oscar Klein was one of the first to do calculations using the Dirac equation. In 1929 he looked at the probability of reflection of an electron from a steep potential barrier supplied by an electric field. He and others found that the probability for reflection exceeded 1 for electric fields beyond $m^2c^3/e\hbar$, i.e. when the field is so high that an electron transported over a Compton wavelength yields mc^2. In a simplifed version in one dimension, the wavefunction of the electron in the domains $V = 0$ and $V = V_0$ with $E^2 = p_x^2c^2 + m^2c^4$ and $(E - V_0)^2 = p_x'^2c^2 + m^2c^4$ giving

$$p_x'^2c^2 = p_x^2c^2 + (E - V_0)^2 - E^2 \tag{11}$$

is

$$\psi(x,t) = \exp^{i(p_x'x - Et)/\hbar} \tag{12}$$

For sufficently small values of V_0, p_x' in eq. (11) is real and there are transmitted waves, eq. (12). For larger values of V_0, p_x' becomes imaginary meaning total reflection, while for values of V_0 exceeding $E + mc^2$ p_x' again becomes real and waves are transmitted. A more careful analysis shows that the potential V_0 must exceed mc^2 in less than a Compton wavelength.

Nowadays, this process is understood as pair production, which - without knowledge of the positron - was an impossible conclusion for Klein and it is therefore known as the Klein paradox. Klein-like pair production is as discussed above addressed in heavy ion collisions where the local field during the collision may becomes 'supercritical' resulting in pair production [30].

Lately, the interest in the Klein paradox has been revived through theoretical studies with wave-packets [47] and space-time resolved simulations [48] that reach very different conclusions concerning the probability of positron production by electrons, $e^- \rightarrow e^-e^+e^-$ so-called trident production, in a strong field. In [48] it is e.g. claimed that 'the incoming electron suppresses the pair production' and we propose to experimentally test such a claim.

Due to the invariance of the parameter $\chi = \gamma\mathcal{E}/\mathcal{E}_0$, it is possible to probe field strengths of the order of those relevant for the Klein paradox in single crystals. The only difference in the three dimensionless invariants describing the problems of trident production in crystals and the Klein paradox is that in the latter case Ξ - expressing the 'inherent' field strength - is of the order one. The relation $\chi \gg \Xi, \Gamma$ still holds for both cases.

In fact, calculations of the drastic increase of trident production in crystals compared to an amorphous material has been existing for more than two decades [49]. One result is shown in fig. 2. Trident production in crystals is 'doubly enhanced' - the emission of the (virtual) photon is enhanced and the subsequent conversion of this photon into a pair is enhanced as well. For low energies the conversion and therefore the pair production enhancement is exponentially suppressed, $\propto \exp(-8/3\chi)$. For intermediate energies, i.e. when $\chi \approx 1 - 10$ the enhancements are each roughly proportional to their respective formation lengths, i.e. to $E(E - \hbar\omega)/\hbar\omega$ and $\hbar\omega$ and for high energies $\chi \gg 1$ the effects are again suppressed ($\propto \chi^{-1/3}$). This qualitatively explains the calculated values shown in fig. 2.

For an electron in a constant electromagnetic field characterized by equation (1), Erber [50] calculated the rate (number per electron per length unit) of trident production by the Weizsäcker-Williams method to be

$$R = \frac{0.32}{\pi}\frac{\alpha^2}{\lambda_c}\frac{\chi}{\gamma}\Omega(\chi) \tag{13}$$

where

$$\Omega(\chi) = \int_0^\infty \frac{1}{u^2}W(\frac{u}{\chi})K_{1/3}^2(\frac{4}{3u})du \tag{14}$$

and

$$W(x) = xK_0(x)K_1(x) - \frac{\chi^2}{2}[K_1^2(x) - K_0^2(x)] \tag{15}$$

In the main region of interest here, $0.1 \lesssim \chi \lesssim 10$, equation (14) is well approximated as

$$\Omega(\chi) = \frac{\pi^{5/2}}{16}(3\chi)^{1/4}\exp(-8(3\chi)^{-1/2}) \tag{16}$$

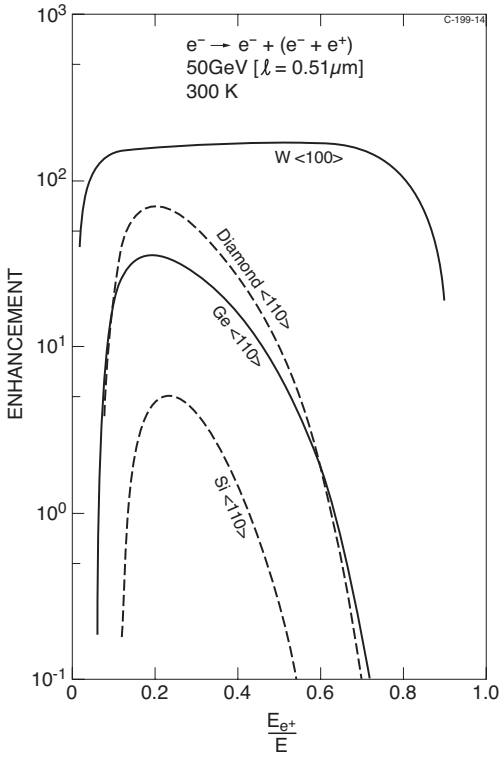

Figure 2: *Enhancement of aligned over random incidence for trident production of four different crystals. The electron energy is 50 GeV and the horizontal scale is the fractional energy taken by the positron. Adapted from [49].*

from which it is seen that the coherent contribution to the trident production is exponentially small for small values of χ, see figure 3, whereas for large values of χ equation (14) tends to $(\pi^2/2)\ln(\chi)$. This logarithmic contribution to the rate, however, requires values of χ exceeding $\simeq 50$ to verify and is beyond present experimental capabilities that are limited to $\chi \lesssim 10$.

As an estimate of χ, we can use the approximate value $\chi_s \simeq 5.2$ for an electron of energy 180 GeV in W along the $< 111 >$ axis [9]. Using equation (13) this translates into a rate of $6.8 \cdot 10^{-3}$ tridents per incident electron in a target of 0.1 mm thickness. However, this calculation assumes a homogeneous field, i.e. it would be expected to underestimate the actual yield in a crystal where the local values of χ can be much higher than χ_s.

Erber [50] also calculated the virtual and real intermediate photon contributions to the trident production in a strong electromagnetic field, $N_V^{(T)}$ and $N_R^{(T)}$, as well as for amorphous materials, $\overline{N}_V^{(T)}$ and $\overline{N}_R^{(T)}$. Defining the enhancement derived from these expressions as $\overline{\eta} = (N_V^{(T)} + N_R^{(T)})/(\overline{N}_V^{(T)} + \overline{N}_R^{(T)})$ we can get an estimate of the total enhancement expected as a function of the local value of χ. This is shown in figure 4, where it can be seen that even for values $\chi \lesssim 10$, the total enhancement can be substantial.

4.2 Experimental details

A measurement of the trident production process requires the use of several thicknesses of foils, since the additional process where the electron radiates a *real* photon that subsequently produces a pair depends on the square of the thickness whereas direct trident production has a linear dependence. Furthermore, the ratio of probabilities for trident production to that of the cascade process involving a real photon in the intermediate step can be estimated as the ratio of the formation length to the target thickness, $l_{\rm f}/\Delta t_f$ [9] such that the required foil thickness must be of the order one formation length. This is a rather modest thickness - even for a 250 GeV electron producing a 1 GeV pair it is 0.1 mm, but it is still possible to discern the signal from background effects, in particular because of the huge enhancement

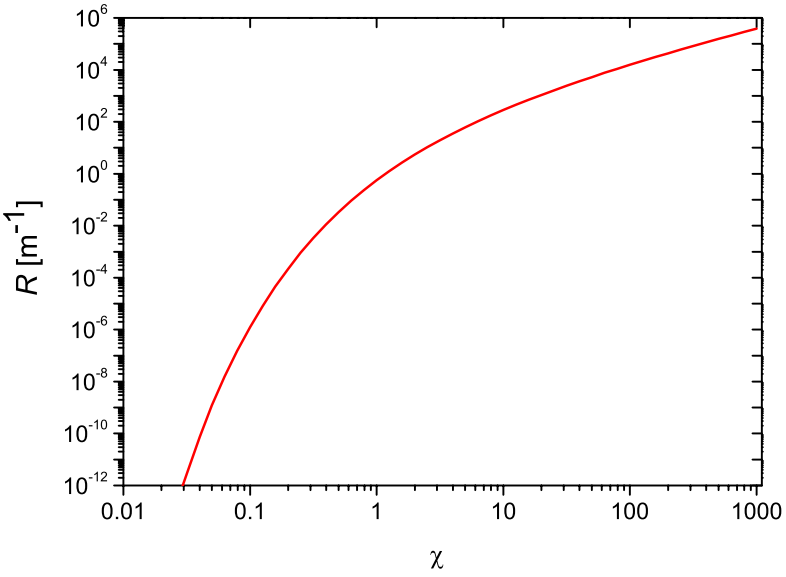

Figure 3: *Rate of trident production as a function of* χ *with* $E = 180$ *GeV, following [50].*

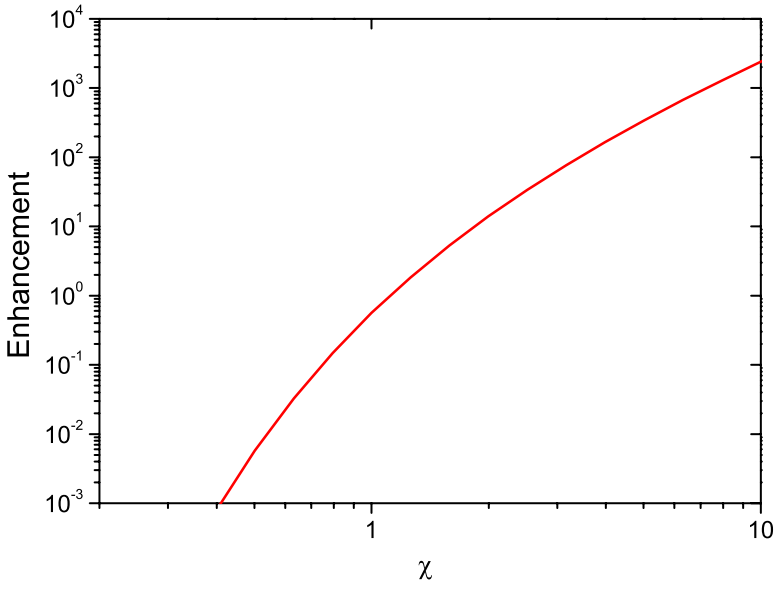

Figure 4: *Enhancement of trident production as a function of* χ *in 100* μ*m W, following [50].*

and the fact that it increases with increasing energy of the primary electron.

A rough estimate of the expected enhancement can be obtained assuming an enhancement in W of 200 found from figure 2 at $E_{e^+}/E = 0.2$ and setting $E_{e^+}/E \simeq E_{e^-}/E$ to give $l_{\rm f}/\Delta t_f \simeq 0.2$. In figure 2 only the W curve is calculated for electrons sufficiently far into the strong field regime ($\chi \simeq 1.5$) to be relevant for a $\simeq$200 GeV beam in Si, Ge or W. Scaling the enhancement η according to formation lengths in units of thickness then shows that the enhancement can be quite large, for example about a hundred for a symmetric pair of total energy 4 GeV generated from a 178 GeV electron in 0.1 mm W. This again

compares well with the calculation of Erber shown in figure 4 where for $\chi \simeq 5$ relevant for 178 GeV electrons in tungsten, a total enhancement of a few hundred is found. Scaling the amorphous yield found with 0.1 mm Cu for pairs $E_{e^+}, E_{e^-} > 1$ GeV by Z^2 we obtain η·2000 trident events per 1e6 incident electrons. Simulations using GEANT show that for every 10^6 electrons penetrating an amorphous Cu target of 0.1 mm thickness, there will be about 300 trident events fulfilling the requirement $E_{e^+}, E_{e^-} > 1$ GeV for detection in a magnetic pair spectrometer based on drift chambers. Using a 0.1 mm thick tungsten crystal in the 'random' orientation increases this number to about 2000, i.e. about 50k events per day taking 50k electrons per burst, a duty factor (50%) and detection efficiencies (35%) into account. This number compares relatively well with the estimate of amorphous trident production in 0.1 mm W by Erber [50] which gives 0.016 tridents in total per electron. Thus, a relatively modest enhancement of trident production of 10% above the random value is expected to be detectable.

An alternative route to estimate the number of trident productions is to approximate the interaction in the crystal as if taking place in a constant field, following the approach of Erber [50].

Even with a pessimistic average η of 2, we get a rate of $4 \cdot 10^{-3}$ trident events per electron. Large enhancements - in principle due to the enhancement of *both* processes of virtual photon emission and pair production - should thus be relatively easily detectable.

Trident production of muon pairs in crystals may turn out to be an efficient method for generating muon beams of low emittance, but in this case the process is not doubly enhanced since only the electron emitting the intermediate (real or virtual) photon emission fulfills $\chi \simeq 1$.

Since the characteristic angle for strong field effects in crystals given by equation (9) is of the order 0.5 mrad for W and Ir, requirements on crystal quality, e.g. the mosaicity, is not as severe as for experiments based on channeling phenomena. Tungsten and iridium crystals with mosaic spreads of the order 0.1 mrad are commercially available.

In the pair spectrometer used by NA43 to detect e.g. photon multiplicities the minimum photon energy was around 5 GeV. The acceptance is given in figure 5 where a Monte-Carlo simulation has been performed which includes details of the drift chambers and the photon energy reconstruction. We intend to use a similar setup, but with the spectrometer magnet run at a lower integrated field to displace the sensitive region towards lower values of the pair or photon energy. For the investigation of trident production itself, the MBPL is to be set to zero field and the desired interaction takes place in the second target position (marked 'Goniometer with crystal in figure 19). However, for the same settings we have the option of turning the MBPL on to measure the photon-initiated pair production for exactly the same setting of the crystal and therefore to have a direct measurement of the real photon contribution.

Since the primary electron remains energetic for the events of main interest, $E_{e^+}, E_{e^-} \gtrsim 1$ GeV, it will be deviated only slightly by the MDX dipole and continues to the nearly forward calorimeter. The adjacent calorimeter blocks are to be used in combination with the information on momentum from the spectrometer.

4.3 Requested beam time

We assume a rate as estimated above of $2 \cdot 10^{-3}$ trident events per incident electron in 0.1 mm W, oriented in the 'random' direction where it behaves as an amorphous foil of thickness $\simeq 3\% X_0$. The typical background radiation from drift chamber windows, scintillators and air-gaps corresponds to slightly less than $1\% X_0$, estimated from previous runs in H4 and H2. Aiming for a total of 1e5 events with $E_{e^+}, E_{e^-} > 1$ GeV, a run in the 'random' orientation requires 5e6 electrons. Using a pessimistic down-time of 50% of the accelerator-chain and counting 4 bursts a minute with 50k electrons, this target takes about 5 hours to complete satisfactory statistics. A run with an oriented target, however, takes considerably longer, since the statistics must allow for off-line angular selections in position and angle. Two oriented crystals of 0.1 mm and 0.05 mm is thus estimated to be necessary to run for a total of 6 days. Since alignment takes about 12 hours for each, two crystals can be investigated in about 7 days of running time.

A full measurement is expected to be possible with about one week of beam time, excluding time for setting up, orienting crystals and calibrating the equipment (estimated on the basis of past experience to take about one week).

We estimate the risk of failure of this sub-project to be relatively modest although there are many

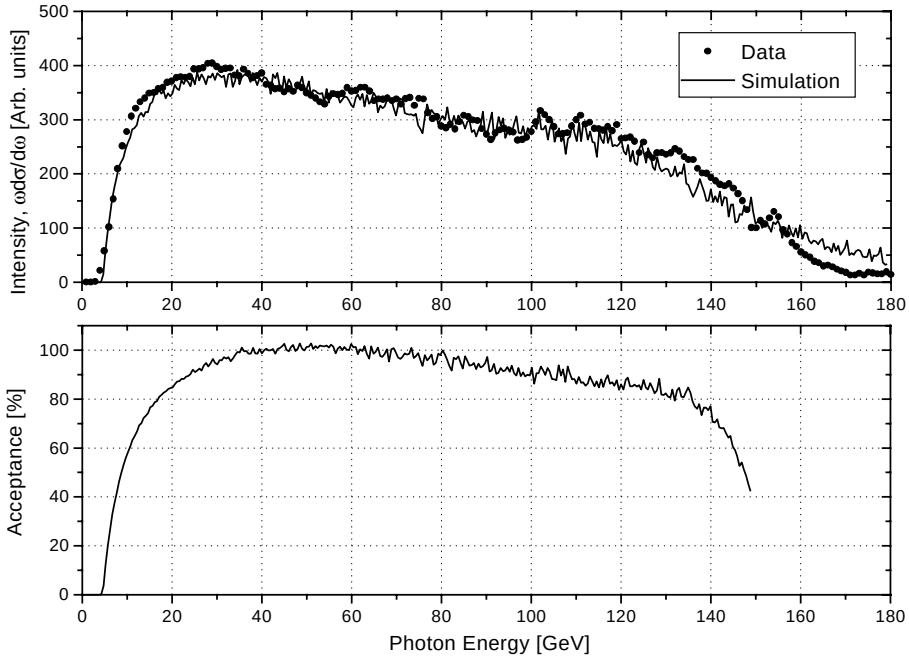

Figure 5: *a) Monte-Carlo simulation compared to data taken by NA43 for the photon energy reconstruction. b) The derived acceptance of the pair spectrometer.*

detectors to be deployed and tested before the actual measurement can be done.

5 Crystalline Undulator

5.1 Theory

Deflection of heavy charged particles in a bent crystal, where the centripetal force is supplied by the 'smeared' field of the screened lattice nuclei, is possible under channeling conditions. In this case, a crystal may deflect the beam as if it were a magnetic dipole of several thousand tesla.

This effect has been proposed to generate a crystalline undulator by application of a transverse acoustic wave to the crystal whereby its fields are bent into a shape resembling that of an ordinary undulator. This is the so-called 'Acoustically Induced Radiation' (AIR) which has hitherto not been observed experimentally [51].

Alternative methods to obtain the shape of an undulator in a crystal have also been proposed, e.g. graded composition strained layers arranged in a superlattice.

5.1.1 Bent crystals for deflection

Although the subject of particle deflection by means of bent crystals is now considered mature and is applied at several high energy laboratories over the world, there are recent developments which expand the region of applications. One such novelty is the extension of the field into the regime of low energy particles. This requires very thin crystals due to dechanneling and has been done by use of a graded composition strained layer. The basis of such layers is the mixture of two materials with different lattice constants as e.g. $\mathrm{Ge}_x\mathrm{Si}_{1-x}$ where the content x of Ge can be varied to produce strain in the crystal which will then bend accordingly. By this method, deflection of 3 MeV protons through an angle of 5 mrad has been demonstrated using a 200 nm $\mathrm{Ge}_{0.15}\mathrm{Si}_{0.85}$ layer on a Si substrate [52]. The time estimated to grow a 1 mm thick $\mathrm{Ge}_x\mathrm{Si}_{1-x}$ crystal with a specified content of Ge can be as little as 1 week although to obtain nearly perfect specimens the growth-time may be substantially higher, about 5Å/s corresponding to about three weeks for a 1 mm crystal [53].

Let us recapitulate the behaviour of a charged particle channeled in a curved crystal: Since the centrifugal term lowers the potential barrier at the outside plane, there is a certain curvature at which the potential minimum is reached at the distance x_c from the plane where the particles will dechannel. An estimate of this curvature can also be based on the centripetal force supplied by the maximum field gradient in the crystal such that for curvatures fulfilling:

$$\kappa \leq \kappa_c = \frac{\pi Z_1 Z_2 e^2 N_c d_p}{pv} \tag{17}$$

the charged particle can channel in a curved crystal. Here, N_c denotes the density of atoms in the crystal, $Z_1 e$ the charge of the penetrating particle, $Z_2 e$ the charge of the lattice nuclei and d_p the planar distance. The dechanneling fraction, i.e. the fraction of initially channeled particles that suffer dechanneling, is roughly given by $F \simeq 3\kappa/\kappa_c$ for small κ, depending e.g. on the initial angular divergence of the beam.

Equivalently, one may fix the maximum curvature by requiring that the bending angle, θ, over one oscillation length in the channel, λ_ψ, must be smaller than the critical angle [54]:

$$\theta(\lambda_\psi) < \psi_p \tag{18}$$

It is clear from eq. (18) that the frequency related to the channeling motion must be larger than that related to the undulator motion for the particle to remain channeled. Therefore, there will always be a separation between the channeling radiation and the (first harmonic of the) undulator radiation. In the following, the layer thickness $h = h_c/4$ has been used, where h_c is the critical layer thickness above which dislocations will tend to relax the strain in the crystal, for details on h_c see [52] and references therein.

Due to the thermal motion of the lattice nuclei in a crystal, the radiation emitted by unbound particles has an incoherent component which is never significantly less than what is obtained from an amorphous material of the same thickness, for a review see e.g. [55]. This is also the case for planar channeled high energy particles where the positively charged ones suffer a slightly decreased total energy loss compared to random incidence. This is, crudely speaking, because the close encounters are suppressed

at the expense of coherence for the soft photon emission such that the high energy photons emitted in incoherent bremsstrahlung are 'shifted' to lower energies [56].

Owing to the requirement on the energy loss, $\Delta E \ll E$, for an undulator, it thus does not make sense to consider crystals with thicknesses larger than about 1/10 of a radiation length. Furthermore, as channeled electrons typically radiate a factor 5-10 more than the incoherent radiation from an amorphous target, crystal thicknesses for undulator applications are in reality limited to much less than 1/10 of a radiation length for electrons. Positrons, on the other hand, lose slightly less energy in total, have a much larger surface transmission - the fraction of incident particles that are initially channeled due to finite divergence and size of the beam - and multiple scatter less due to the steering effect of channeling.

Thus, to obtain several periods in the crystalline undulator the wavelength λ must be quite small, less than a few hundred μm, depending on the material. The restrictions on the curvature given by eq. (17) and the maximum curvature for a sinusoidal wave, $\kappa = A(2\pi)^2/\lambda^2$, lead to

$$pv \leq \frac{Z_1 Z_2 e^2 N_c \lambda^2}{4\pi} \frac{d_p}{A} \tag{19}$$

The condition $A \gg d_p$ is imposed on the amplitude of oscillation in order to reduce interference between channeling radiation and crystalline undulator radiation. This requirement combined with eq. (19) gives $pv \leq 32$ GeV for Si (110) taking $\lambda = 200$ μm (giving $N = 10$ oscillations in a crystal of thickness $X_0/50$ where $\Delta E/E$ is expected to be tolerable), $\kappa = 0.1\kappa_c$ (ie. $F \simeq 0.3$ so about 50% of a completely parallel and optimally aligned beam will channel through one period) and $A = 10d_p$. Heavier materials may be envisaged to increase this limit, but hitherto most applications of bent crystals have used Si or Ge due to their negligible mosaic spread [57].

On the other hand, the (straight crystal) dechanneling length for positively charged particles[1)], L_D, imposes restrictions on the momentum as well since the dechanneling length scales roughly proportional to pv and is barely 1 mm for Si at 2 GeV. For a curved crystal the dechanneling length is shortened to approximately $L_D(\kappa) = L_D(0)(1 - \kappa/\kappa_c)^2$. Furthermore, under a resonance condition channeled particles in a superlattice may suffer so-called 'catastrophic dechanneling' such that the effective channeled particle wavelength, λ_e, should be chosen away from this region, i.e. $\lambda_e \simeq s$, where s is the path length per layer of the superlattice [58].

From the above general arguments:

1. small energy loss $\Rightarrow$ small thickness + given number of periods $\Rightarrow$ small oscillation wavelength + critical curvature $\Rightarrow$ upper limit of energy
2. small dechanneling $\Rightarrow$ given thickness $\Rightarrow$ lower limit of energy

it should be clear that the allowable range of energies to observe the crystalline undulator radiation is around 0.5-20 GeV, irrespective of the method used to generate the curvatures.

We note that the so-called strong field effects mentioned above become significant for planes in heavy crystals already around 100 GeV. Beyond this energy, the effective radiation length decreases rapidly by up to a factor $\approx 400/Z$ such that even positrons lose a substantial fraction of their energy within less than 100 μm [59]. The characteristic angle for the strong field effects is larger than the Lindhard angle for channeling at these energies. It thus seems impossible to use crystalline undulator radiation or AIR above $\simeq 100$ GeV.

Radiation from planar and axially channeled electrons and positrons in the energy range 2-55 GeV/c was investigated already in the mid-80's at CERN [56]. It was found that positrons emit channeling radiation (ChR) with characteristic peaks which scale slightly slower than $E \propto \gamma^{3/2}$ and have a first harmonic of 26 MeV at 5 GeV incident energy. According to the discussion connected to eq. (18) the first harmonic of the ChR, $\hbar\omega_{\mathrm{ChR}}$, is well separated from the crystalline undulator radiation as will also become evident from the table below.

Apart from the crystalline undulator approach, radiation from channeled positrons in bent crystals has been investigated theoretically at 5 GeV [60], but for one circular section only and without considering what mechanisms to apply to make a crystalline undulator.

[1)] The dechanneling length is about an order of magnitude shorter for negatively charged particles compared to positively charged particles.

We are pursuing the fabrication of a passive crystalline undulator by use of graded composition strained layers which vary the composition defined by x in an oscillatory manner to obtain a superlattice of many periods [61]. This approach clearly has the drawback that the oscillation amplitudes and wavelengths cannot be varied after the fabrication of the crystal, but it avoids the difficulties connected to applying a transverse acoustic wave to a thin crystal. Furthermore, as the superlattice is grown on an unbent substrate it is easy to align the entrance face to obtain channeling conditions for the full beam. Also, since the curvature in the channel is proportional to the slope of the x-content versus depth, the curvature for crystalline undulator radiation can be varied through grading the composition according to many different desired shapes, e.g. sinusoidal or saw-tooth.

As discussed above, the crystalline undulator radiation (and most likely also the AIR) is only applicable in the range of about 0.5-20 GeV, where the channeling or strong field radiation does not violate $\Delta E/E \ll 1$ and the dechanneling is not excessive in a crystal thick enough to support many periods.

With a super-periodicity imposed by either ultra-sound [62], strain in Si-Ge interfaces [63] or surface defects [64] the theoretically possible, high-intensity, nearly mono-chromatic radiation from a crystalline undulator [66, 51], is shown in figure 6. A detection of the generated undulator-like radiation will constitute a proof-of-principle of this novel type of 'insertion device'. Again, it is the very strong crystalline fields that boost the photon frequencies to much higher values, see figure 7, while at the same time requiring much less space, of the order few mm.

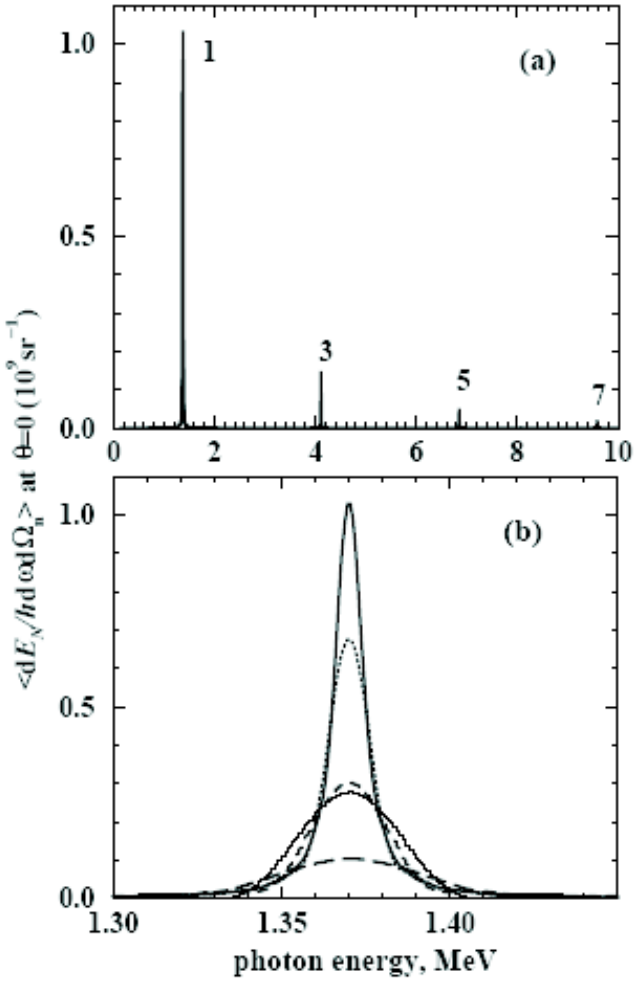

Figure 6: *Theoretical spectral distribution of crystalline undulator radiation in the forward direction for 5 GeV positrons channeled in a 3.2 mm thick Si (110) crystalline undulator with $N_d = 51$ periods. In (b) is shown the profiles of the first harmonics for $N = 4N_d$ (solid), $N = 2N_d$ (dots), $N = N_d$ (dash), $N = N_d/2$ (long-dash). Adapted from [67].*

	2 GeV/c	10 GeV/c
$\hbar\omega_{\max}$	718 keV	17.9 MeV
$\hbar\omega_{\mathrm{ChR}}$	7 MeV	57 MeV
p_{u}	1.89	5.51
A	38 Å	65 Å
$x_{\max}$	1.3%	0.77%
N	20	27
κ_c/κ	5.0	5.0
N_{ω_K}	1.5	2.0
$\hbar\omega_1$	274 keV	402 keV
θ_0	0.34 mrad	0.20 mrad
$\Delta\omega/\omega$	0.10	0.073
L_D	0.87 mm	3.99 mm
Δt	1 mm	4 mm
$\Delta E/E$	1.1%	4.1%
ψ_p	114 μrad	51 μrad

Table 1: *Parameters for the graded composition strained layer crystalline undulator for positrons of 2 and 10 GeV/c in a Ge_xSi_{1-x} crystal of thickness Δt aligned on the (110) plane. The numbers are given as described in the text.*

In table 1 we present results of calculations performed as in [51] for two cases (from [63]). The table shows the maximum photon energy, $\hbar\omega_{\max} = p_{\mathrm{u}}\gamma^2\hbar\omega_0$, when the undulator parameter, $p_{\mathrm{u}} = 2\pi\gamma A/\lambda$, is larger than 1, the first harmonic of the channeling radiation, $\hbar\omega_{\mathrm{ChR}}$, the oscillation amplitude, A, the maximum Ge content, $x_{\max}$, the number of periods, N, the fixed curvature in units of the critical curvature, κ_c/κ, the number of photons emitted per positron, $N_{\omega_K} = 8\pi\alpha N 2^{-4/3}$, and their first harmonic energy, $\hbar\omega_1 = 4\gamma^2\hbar\omega_0/p_{\mathrm{u}}^2(1 + 2/p_{\mathrm{u}}^2)$, the emission cone, $\theta_0 = p_{\mathrm{u}}/\sqrt{2}\gamma$, the energy spread, $\Delta\omega/\omega = 2/N$, the dechanneling length, L_D, the crystal thickness, Δt, the fractional incoherent energy loss, $\Delta E/E$, and the planar critical angle in (110) Si, ψ_p.

The cases studied are 2 GeV positrons in a 1 mm thick crystal with $x_{\max} = 0.013$ and $N = 20$ and 10 GeV positrons in a crystal of larger thickness with $x_{\max} = 0.0077$ and $N = 27$. Although it is advantageous to use positrons to generate radiation (because of decreased multiple scattering under channeling conditions) [51], we wish as well to investigate the behaviour of electrons. With a week of beam time for this sub-experiment, we would be able to run with two different crystals, testing the different approaches to produce a crystalline undulator, with both positrons and electrons, and for several energies. We are presently studying methods to develop $Si_{1-x}Ge_x$ crystals by means of Molecular Beam Epitaxy.

As shown in table 1 and seen in simulations [65], the interesting photon energies from the crystalline undulator appear near the annihilation peak at 511 keV. Simulations performed using GEANT, see figure 8, show, however, that using a $2'' \times 2''$ germanium detector, the disturbing effect of the annihilation radiation originating from pairs generated in the surroundings by the unavoidable channeling radiation, is sufficiently small or can be reduced to a negligible level. For comparison, in the vicinity of the first harmonic of the channeling radiation, the number of photons emitted per positron is about $4 \cdot 10^{-4}$/MeV [63].

5.2 Experimental details

The proposed structure of the experimental setup for the investigation of radiation from crystalline undulators is shown in figure 20. Its main components are 3 drift chambers, (DCs) for the definition of the entry- and exit-angles and positions on the target. Downstream the MBPL where the primary e^+/e^- are deflected, a He-tank is positioned to reduce the conversion probability of the photons. Finally, the photons are intercepted by a downstream calorimeter, consisting of either NaI or $LaCl_3$(Ce) crystals. The spent lepton is absorbed in a dump constructed from iron and lead blocks.

The principle of construction for the crystalline undulators is summarized in figures 9 and 10. The

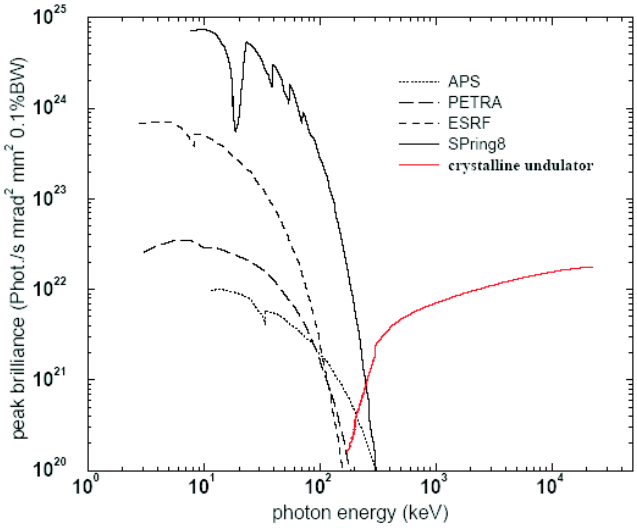

Figure 7: *Peak brilliance of crystalline undulator radiation in the forward direction (red line) compared to conventional third generation light sources as indicated. From [68].*

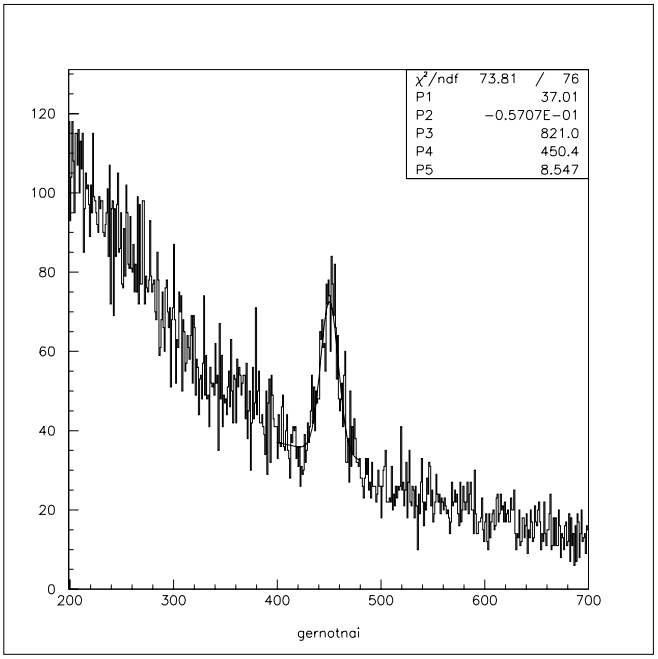

Figure 8: *Simulated values for the detection of 450 keV crystalline undulator radiation with intrinsic energy spread* $\sigma/E = 0.02$ *in a* $2'' \times 2''$ *germanium detector. The absence of 511 keV annihilation gammas from the surroundings is achieved by means of an anti-Compton detector, a* $5'' \times 5''$ *NaI.*

trench of typical size 10 μm - produced by either mechanical means or laser ablation, imposes a strain in the crystalline lattice. This strain deforms the lattice to depths of hundreds of microns in the crystal and by implementing these trenches on both sides of the crystal, the crystallographic planes oscillate as a function of position.

One example is shown in figure 11 where the bending device is present to diminish the effect of so-called anticlastic bending, a result of having trenches on one side of the crystal only. At the time of writing, laser ablation techniques are being developed to make cleaner and more homogeneous trenches, and to obtain trenches on both sides of the crystal with a spacing definition to better than a few μm.

A short test performed during the 'Chudakov' experiment in H4 at the end of 2004 showed that crystals as the one shown in figure 11 are possible to align using a 150 GeV electron beam. The angu-

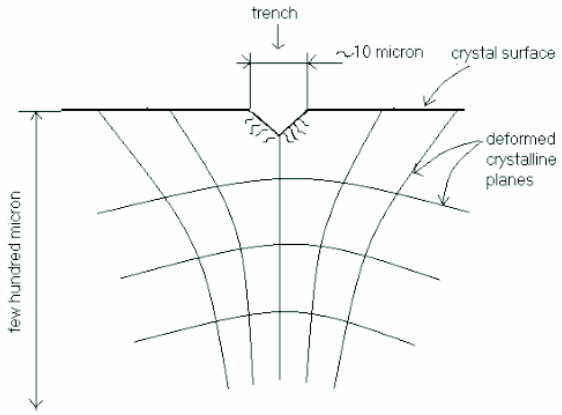

Figure 9: *Drawing of the propagation of deformation into the bulk of a single crystal as a result of a mesoscopic surface defect.*

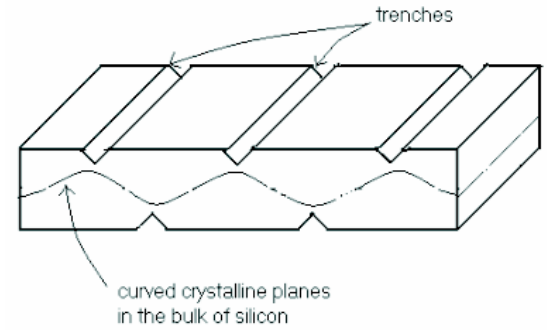

Figure 10: *Drawing of the principle of converting the phenomenon shown in figure 9 into a crystalline undulator.*

lar width of the alignment scans was as expected and alignment scans are fast due to this width being proportional to the amplitude of angular oscillations in the crystal, i.e. about half a mrad. Alignment is thus expected to be possible in a few hours of beam time for each crystal. However, this test also showed that due to the transversely very thin target, the signal-to-noise ratio S/N was a challenging problem. Alignment with 10 GeV positrons showed only $S/N \simeq 4\%$ and most of this small enhancement was likely to be due to channeling radiation, not the sought crystalline undulator radiation. Moreover, Compton scattering of high energy photons contributes a significant background in the photon energy region of interest. These problems will be overcome by means of tight event-selections on-line provided by narrow slit-scintillator counters as well as off-line by cuts on beam profiles using the drift chambers. An additional scintillator counter to be included as a 'radiation event trigger' may be inserted just upstream the dump, to flag those particles that have suffered little energy loss.

5.3 Requested beam time

The focus of this experiment is the emission of very low energy photons (MeV region). Thus, essentially all positrons accepted by the primary trigger ($\mathrm{Sc1} \cdot \mathrm{Sc2} \cdot \overline{\mathrm{Sc3}}$) are good events. On the other hand, in order to be able to set upper limits on the efficiency of the actual mechanism of emission of crystalline undulator radiation - if not observed - good statistics is needed. Aiming for 100 bins in the interval 0.1-5 MeV (to get 10% energy resolution at 511 keV), each with a 1% error bar this means about 1e6 events in total per target. An additional factor of 3 allows for angular selections in the off-line analysis, corresponding to about what the drift chamber resolution allows. Accepting 2000 events per burst, using a pessimistic down-time of 50% of the accelerator-chain and counting 4 bursts a minute,

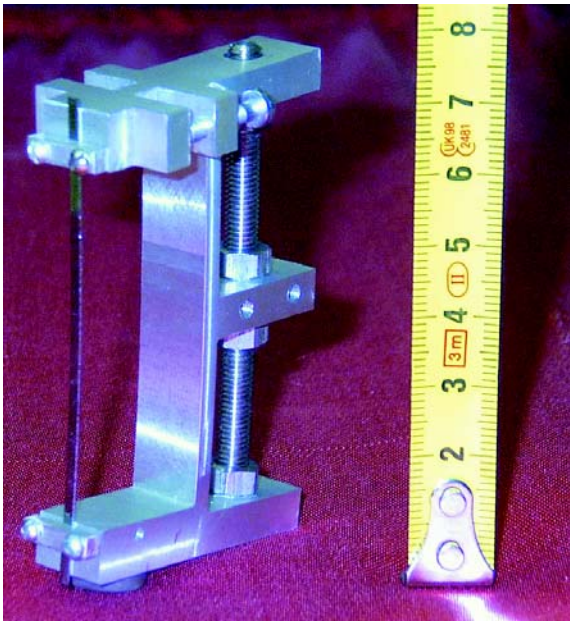

Figure 11: *A picture of one of the available 'trenched' crystalline undulators, mounted in its holder.*

each target takes about 12 hours to complete a satisfactory statistics.

Initially, we propose to measure with a mechanically manipulated ('trenched') undulator crystal, an identical crystal without 'trenches', a $Si_{1-x}Ge_x$ MBE grown strained lattice crystal, a pure Si crystal of similar dimensions and an extended run without target. With these runs, taking change-over time, alignment and calibration verification inbetween runs into account, this experiment is estimated to take 5 days. Given that this investigation becomes succesful, we propose a more in-depth investigation of the phenomenon, varying parameters such as the positron energy, oscillation wavelength and amplitude and testing with electrons.

We estimate the risk of failure of this sub-project to be not insignificant, but with a similarly high scientific potential. There are alignment procedures that have proven operational in the previously performed test, but signal-to-noise ratios must be improved compared to that test to ensure a fast and precise alignment at 10 GeV. This enhancement in performance is likely to be achieved by means of drift chambers (which were not used previously) and custom-made veto-scintillators for the thin targets, as well as the fabrication of a large target (a 4 inch wafer) based on the $Si_{1-x}Ge_x$ MBE grown strained lattice. The setup consists of detectors that from previous runs are known to be reliable and predictable.

Finally we are investigating the potential of using laser-ablated diamonds instead of silicon. The advantage of this is the extremely high radiation hardness of diamonds, known e.g. from tests at the Final Focus Test Beam at SLAC. This superiority is the result of two properties of diamond: The very tight lattice, i.e. the small lattice constant, and a thermal conductivity which exceeds that of most other materials by three orders of magnitude. For a future investigation approaching the theoretically possible lasing regime of such undulators which requires beam densities of the order $10^{20}/\mathrm{cm}^3$, radiation hardness will be of utmost importance.

6 Axial and planar investigations of spin-flip radiation

6.1 Theory

The effect of spin on the radiation for near-critical magnitudes of the field in the rest-frame of the emitting electron has been tested only in the axial case and for a relatively thick crystal. This may be extended to investigate planar effects as well as axial for thin crystals. The planar case for positrons is much more well-defined since the number of initially channeled particles is high, about 90% as opposed to barely 5% for axially channeled electrons.

Asymptotically, the spin contribution becomes $\xi dN/d\xi \propto (\xi^7/(1-\xi))^{1/3} \cdot \chi^{2/3}$ for $\chi \to \infty$ such that it is strongly peaked at the upper end of the spectrum. An example is given in fig. 12 where the value of χ is set to 100.

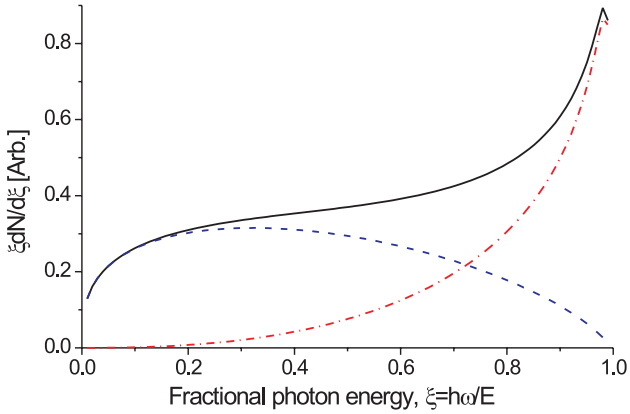

Figure 12: *Synchrotron radiation in a strong field, where the full line is the total spectrum, the dash-dotted line shows the contribution from the spin and the dashed line is obtained by neglecting the spin as in [13]. The value of χ is set to 100.*

The study of radiation emission for high values of χ is relevant for e.g. beamstrahlung. The emission of beamstrahlung can be expressed as a function of χ which for the Stanford Linear Collider (SLC) is small $\simeq 10^{-3}$ but of the order unity for the next generation linear colliders [69, 70]. The influence of spin on the radiation process [6, 35] becomes the dominant factor once χ becomes much higher than 1. We wish to do a measurement in two 'cleaner' cases, namely where the crystal is thin enough to make pile-up insignificant as well as by using a pair spectrometer to 'deconvolute' the photon spectrum into its single photon components. Furthermore we intend to study the case of planar channeled positrons, where the transverse potential is well approximated by a harmonic potential.

For a future linear collider operating in the 'quantum regime', the beamstrahlung spectrum becomes similar to the spectrum shown in fig. 12, see the full-drawn line in fig. 13.

6.2 Experimental details

This experiment requires aligned thin crystals of heavy elements like tungsten or iridium as well as the operation of 4 drift chambers for angular and position selections on the crystals as well as photon tagging. We aim to produce 'single-photon spectra' by means of reconstruction of the photon momentum in a magnetic pair spectrometer. This spectrometer - which is based on conversion of the photons into electron-positron pairs and subsequent magnetic momentum analysis, see figure 21 - has been operated before by NA43. It is sufficient to use a MDX dipole magnet in combination with two drift chambers.

6.3 Requested beam time

As the crystals must be aligned to an axial orientation, the alignment procedure - even with a pre-aligned crystal - is expected to take about half a day for each crystal. The most important region of emission is the high energy photons, i.e. $\xi \gtrsim 0.6$. In 0.1 mm W, oriented in the 'random' direction where it behaves as an amorphous foil of thickness $\simeq 3\% X_0$, the fraction of photons emitted above

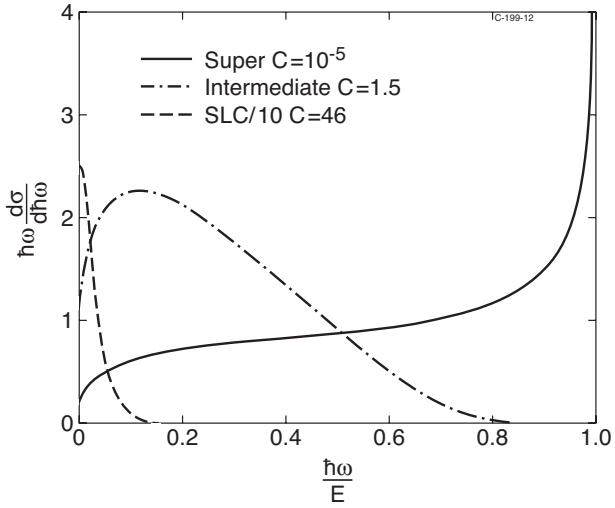

Figure 13: *Three examples of beamstrahlung power spectra where the horizontal scale is the fractional photon energy and the constant C here is approximately equal to $1/\chi$. Adapted from [71].*

$\xi = 0.6$ is 1.4% of the number of incident electrons. The typical background radiation from drift chamber windows, scintillators and air-gaps corresponds to slightly less than 1%X_0, estimated from previous runs in H4 and H2. Aiming for a total of 5e4 events with $\xi > 0.6$, a run in the 'random' orientation requires 7e6 electrons. With a total reconstruction efficiency of tracks through the magnetic pair spectrometer of about 50% in this energy region (highly asymmetric pairs where e.g. the positron takes more than 90% of the energy cannot be detected), and a conversion efficiency of the photons to detectable pairs of 10% (must be kept relatively low to avoid radiation generated by the pair) 140e6 electrons are needed. Using a pessimistic down-time of 50% of the accelerator-chain and counting 4 bursts a minute with 50k electrons, this target takes about 24 hours to complete satisfactory statistics. A run with an oriented target, however, takes considerably longer, since the statistics must allow for off-line angular selections in position and angle. Two oriented crystals of iridium and tungsten is thus estimated to be necessary to run for a total of 7 days.

We estimate the risk of failure of this sub-project to be relatively modest although there are many detectors to be installed and tested before the actual measurement can be done.

7 Pair production and radiation emission in heavy crystals at few tens of GeV

7.1 Theory

Following the succesful experimental test in H2 of the Landau-Pomeranchuk-Migdal (LPM) effect at high energies [17, 18], we wish to study the formation process of high energy photons and pairs. The basis of the LPM effect is the 'formation length' - the distance traversed by an electron during the emission of the photon [7]. The formation length can be up to 100 microns, depending on electron and photon energy. Low energy photons have longer formation lengths.

The LPM suppression in pair production for presently available accelerator energies is negligible. Even for a near future few-TeV electron beam generating TeV bremsstrahlung photons, an experimental assessment would be extremely demanding. Comparing the yield of the central, symmetric pairs which suffer the strongest suppression, the numbers are reduced by about 1 % from the Bethe-Heitler limit to the LPM suppressed yield at 1 TeV. At 10 TeV the corresponding number is 14 %, see e.g. [72]. However, crystals may present a possibility for measuring LPM suppression in pair production with beams in the few-hundred GeV region available today. The main reason is that the photon conversion into pairs in an aligned crystal predominantly takes place where the field is strongest, i.e. at small transverse distances from the string of nuclei. At this transverse location, also the multiple Coulomb scattering is drastically increased - by up to three orders of magnitude. Therefore, one may expect the threshold for LPM suppression to decrease by approximately the same three orders of magnitude corresponding to a replacement of TeV by GeV. However, it is only the incoherent contribution that becomes suppressed and since the coherent contribution quickly dominates the pair production cross section, the strong incoherent suppression becomes a small correction to the total yield, except near the threshold for strong field effects where the incoherent contribution plays a significant role [8, 19]. Thus, accurate experimental studies of the pair creation by photons of energies in the few-tens of GeV range, is a possible route to investigating the LPM effect in pair production, a route that would otherwise require multi-TeV beams in amorphous media, see figure 14.

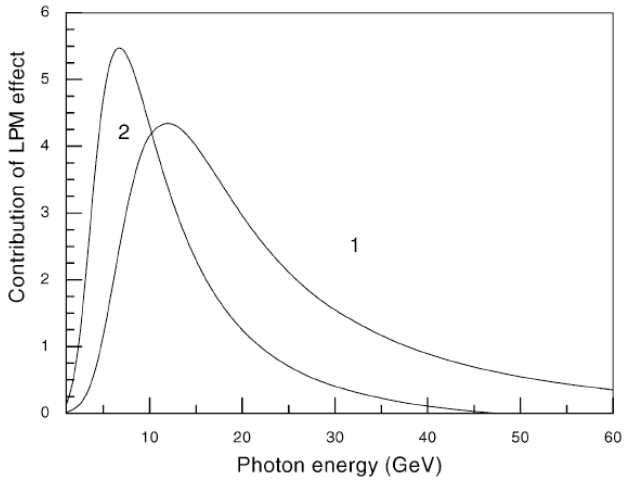

Figure 14: *The relative contribution of the LPM effect Δ (in percent) in tungsten, axis $< 111 >$. Curve 1 is for T = 293 K and curve 2 is for T = 100 K. From [8].*

Furthermore, accurate experimental results for both radiation emission and pair creation in heavy crystals (tungsten, iridium) are desirable to test the accuracy of the main theoretical approach in the field, the so-called Constant Field Approximation developed by Baier's group. For the potential use of single crystals in high energy physics or astrophysics for e.g. calorimetry [73, 46] or for the simulations of extended air showers, an assessment of the theoretical accuracy is necessary.

7.2 Experimental details

This experiment can be run in combination with 'Axial and planar investigations of spin-flip radiation', but requires the installation of an additional goniometer stage downstream the MBPL dipole

magnet that separates the spent electron from the photon beam, see figure 22. This second crystal must be aligned to an axial orientation and we have the option on this goniometer stage to provide cooling to $\simeq 100$ K by liquid nitrogen.

7.3 Requested beam time

This experiment only requires supplementary beam time through the need for a longer sequence of orientations of the second crystal. It is highly desirable to control the amount of averaged multiple scattering - and therefore the influence of the LPM effect - by a comparison of several runs as a function of angle to the axis. As a minimum, an exact angular orientation and an orientation at half a critical channeling angle and at half a strong field angle is required. Each of these settings will take about 12 hours to complete, i.e. about 3 additional days in total, including alignment of the second crystal.

We estimate the risk of failure of this sub-project to be at about the average level of the proposed experiments. There are many detectors to be installed and tested. Systematic effects like angular drifts of the crystals during the long exposure times (e.g. by mechanical instabilities or temperature variations) may affect the outcome, but is under control, judging from experience based on previous runs.

8 Sandwich (structured) targets

8.1 Theory

In the bremsstrahlung emission from an energetic positron or electron traversing a solid, there are four basic scales of length: The radiation length, X_0, the foil thickness, Δt, the formation length $l_{\rm f} = 2\gamma^2 c(E - \hbar\omega)/E\omega$ and the 'multiple scattering length', $l_\gamma = \alpha/4\pi \cdot X_0$, where $E = \gamma mc^2$ and $\hbar\omega$ are the energy of the positron and photon, respectively, m is the rest mass of the positron, γ the Lorentz factor, α the fine-structure constant and c the speed of light. Of these lengths, the only one that depends on photon and particle energy is the formation length, whereas the other lengths depend on the target material or shape.

The earlier papers [17, 18], measurements of the Landau-Pomeranchuk-Migdal (LPM) effect performed in H2 at CERN were presented - a suppression of radiation yield from electrons with energies in the few-hundred GeV range. The LPM effect can as discussed above be interpreted as a disturbance of the projectile within the formation length that leads to a reduced radiation probability. In other words, the suppression appears if the formation length exceeds the multiple scattering length, but remains smaller than the target thickness, i.e. $l_\gamma < l_{\rm f} < \Delta t$. Since the formation length is inversely proportional to the energy of the radiated photon, low energy photons suffer a stronger suppression than high energy ones for fixed energy of the particle. Furthermore, for particle energies of around 200 GeV, the formation length for a 20 GeV photon becomes a few microns long, i.e. in the experimentally accessible regime for the experimental use of thin targets in high energy beams like the H2 or H4 beams of the SPS. Likewise, for heavy materials the multiple scattering length becomes a few microns. In experiments performed at SLAC, the case $l_\gamma < \Delta t < l_{\rm f}$ has been studied [74, 75, 76] where the formation length loosely speaking extends out of the target while the target is thick enough to yield a typical scattering angle exceeding $1/\gamma$. In this case, a new type of suppression phenomenon appears, first treated theoretically by Ternovskii [77] and later in substantial detail by Shul'ga and Fomin [78, 79, 76, 80, 81, 82].

The proposed study is aimed at providing an experimental answer to the questions: what happens to formation zone effects once the available target thickness becomes comparable to the multiple scattering length which in turn is smaller than the formation length, i.e. when $l_\gamma \simeq \Delta t < l_{\rm f}$? Theoretically, the target will act as a single scatterer and will produce radiation according to the unsuppressed Bethe-Heitler mechanism even though $l_{\rm f} > l_\gamma$ [81]. Moreover, transition radiation in the multiple scattering dominated regime turns out to give a significant contribution to the radiation in the few-GeV region. Secondly: what happens when the formation length 'bridges the gap' between two or more foils?

The basic formulas for the various radiation effects considered are briefly presented. For more comprehensive discussions the reader is referred to other texts [83, 18].

8.1.1 Landau-Pomeranchuk-Migdal effect

Since the majority of radiation emission takes place within a cone of opening angle $1/\gamma$ to the direction of the electron, loss of coherence during the formation time results in suppression if the electron scatters outside this cone. So if half (in the convention of [83]) the formation length exceeds the length l_γ, the emission probability decreases, i.e. an onset of the LPM effect at energies:

$$\hbar\omega_{\rm LPM} = \frac{E^2}{E + E_{\rm LPM}} \tag{20}$$

where $E_{\rm LPM} = mc^2 X_0/4\pi a_0 = 7.68 \cdot X_0$ TeV/cm and a_0 is the Bohr radius.

The LPM effect in finite size targets was treated theoretically in detail by e.g. Blankenbecler and Drell [84], by Zakharov [85] and by Baier and Katkov [86].

8.1.2 Thin target - Ternovskii-Shul'ga-Fomin effect

Because the formation length for radiation emission increases with decreasing photon frequency, at a certain point the formation zone extends beyond the thickness of the foil. In this case, the radiation yield also becomes suppressed. The phenomenon is also of substantial interest in QCD [87, 88, 89, 91].

For the Ternovskii-Shul'ga-Fomin (TSF) effect, the analysis is applicable for target thicknesses $l_\gamma \ll \Delta t < l_{\rm f}$, see e.g. [81]. Combining the formation length and the target thickness parametrized by

$k_{\rm f} > 1$, $\Delta t = l_{\rm f}/k_{\rm f}$, the effect becomes appreciable for photon energies

$$\hbar\omega < \hbar\omega_{\rm TSF} = \frac{E}{1+\frac{\Delta t}{2\gamma\lambda_c}} \tag{21}$$

where $\lambda_c = \hbar/mc$ is the (reduced) Compton wavelength.

The magnitude of the effect is evaluated from the averaged radiation spectrum [81]

$$< \frac{{\rm d}E}{{\rm d}\omega} > \simeq \frac{2\alpha}{\pi}(\ln(\frac{\Delta t}{l_\gamma}) - 1) \tag{22}$$

and since for the Bethe-Heitler case $< \frac{{\rm d}E}{{\rm d}\omega} >= 4\Delta t/3X_0$, the suppression factor, κ, can conveniently be expressed as

$$\kappa \simeq \frac{k_\gamma}{6(\ln k_\gamma - 1)} \tag{23}$$

where $\Delta t = k_\gamma l_\gamma$ and $k_\gamma \gg 1$ ensures $\Delta t \gg l_\gamma$. As an example, for $\Delta t = 0.3\% X_0$, corresponding to a 10 μm thin Au target and $E = 178$ GeV, $k_\gamma \simeq 5$ yielding a suppression $\kappa = 1.3$ for photon energies lower than $\hbar\omega_{\rm TSF} = 4.7$ GeV.

At higher energies, as the Lorentz factor γ becomes comparable to $\Delta t/2\lambda_c$ the suppression affects a substantial part of the spectrum. At 4 TeV - perhaps relevant for a tertiary electron beam derived from the LHC beam [92] - the effect suppresses the lower half of the radiation spectrum by a factor 2 in a 7 μm thick Au foil. The effect may thus be an alternative to coherent bremsstrahlung from a crystal to enhance the production of high energy photons from a target or, equivalently, to suppress the low energy photon emission. However, if the theory is correct, the suppression should disappear once the target no longer fulfills $\Delta t \gg l_\gamma$ since the radiation will re-enter the regime of the Bethe-Heitler type.

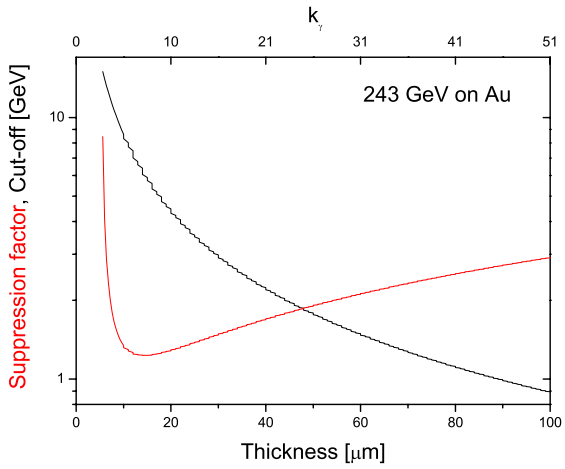

Figure 15: *The suppression factor κ from eq. (23) and the threshold $\hbar\omega_{\rm TSF}$ from eq. (21).*

8.1.3 Transition radiation

Following the discussion in [55] there are two different regimes of emission of transition radiation corresponding to the requirements $E < E_0$ or $E > E_0$ where $E_0 \simeq \omega_p l_\gamma mc$ separates the two regions according to whether or not multiple scattering is important. Here ω_p is the plasma frequency yielding $E_0 \simeq$0.4 GeV for Au where $\omega_p \simeq 80$ eV. In the region $E < E_0$ the number of photons emitted per edge is given by the 'standard' expression (see e.g. [93])

$$\frac{dN}{d\hbar\omega} = \frac{\alpha}{\pi\hbar\omega}[(1+\frac{2\omega^2}{\gamma^2\omega_p^2})\ln(1+\frac{\gamma^2\omega_p^2}{\omega^2}) - 2] \tag{24}$$

while in the region $E > E_0$ the number of photons emitted per edge is given by

$$\frac{dN}{d\hbar\omega} \approx \frac{\alpha}{\pi\hbar\omega}[\ln(\frac{1+\sqrt{1+4\omega_{\rm LPM}/\omega}}{2}) + \frac{2}{1+\sqrt{1+4\omega_{\rm LPM}/\omega}} - 1] \tag{25}$$

which is valid for $\hbar\omega > \gamma\hbar\omega_p$ and a not too thin foil.

These expressions approximately agree for energies smaller than $\simeq 0.1\gamma\hbar\omega_p$ corresponding to 2.8 MeV in Au. For an energy $\hbar\omega = 5$ GeV in 2μm Au, eq. (24) multiplied by $2X_0/\Delta t$, i.e. normalized to thickness and taking entry and exit edge into account, gives $dN/d\hbar\omega = 10^{-11}$ GeV^{-1}. For the same conditions, eq. (25) gives $dN/d\hbar\omega \approx 0.34$ GeV^{-1}. Both conditions $E > E_0$ and $\hbar\omega > \gamma\hbar\omega_p$ are fulfilled by a reasonable margin. This can be compared with an alternative treatment [94] (see also [75]) valid for photon energies $\gamma\hbar\omega_p(\gamma\hbar\omega_p/\hbar\omega_{\rm LPM})^{1/3} < \hbar\omega \ll \hbar\omega_{\rm LPM}$, corresponding to 4 MeV$< \hbar\omega \ll$11.5 GeV in Au

$$\frac{dN}{d\hbar\omega} = \frac{\alpha}{\pi\hbar\omega}\ln(\frac{2}{3}\sqrt{\frac{\hbar\omega_{\rm LPM}}{\hbar\omega}}) \tag{26}$$

which at $\hbar\omega = 5$ GeV yields $dN/d\hbar\omega \approx 0.019$ GeV^{-1}. In fact, [94] shows eq. (25) with different numerical coefficients yielding a lower result $dN/d\hbar\omega \approx 0.22$ GeV^{-1}. Thus, it is not unreasonable to expect that eq. (25) - which is anyway only approximate - may overestimate the yield of transition radiation.

A more recent theory of the multiple scattering dominated transition radiation is provided by Baier and Katkov [86]. Although rather compact, their expression (eq. (4.9) [86]) requires the definition of a number of auxiliary variables. The yield is about a factor 2 higher than that given by eq. (25).

In any case, the analysis shows that transition radiation dominated by multiple scattering may be a necessary ingredient in the description for targets thick enough to yield this type of radiation.

8.1.4 Structured target theory

In Blankenbecler's theory [95, 96] (see also [85]) interference mechanisms are considered for targets of up to 10 segments. It is shown that 'the photon spectrum is clearly developing a peak where the formation length is approximately equal to the distance between the centers of the plates' [95]. Even though these calculations are performed only for 25 GeV (and in a single case 50 GeV), there seems to be no reason to expect that this observation does not apply to the general case.

In [98], Baier and Katkov treat the radiation emission from a stack of thin foils, including the LPM and polarization effect and emission from the target boundaries (transition radiation). For the general case of N foils, however, they only give an explicit formula for the strong scattering, large spacing case where, in their notation, $b \ll 1$ and $T = (l_1 + l_2)/l_{\rm f} \gg 1$, l_1 being the target segment thickness, l_2 the segment spacing (their eq. (2.49)) and $b = \alpha X_0/2\pi l_1$ the scattering variable [2)]. The length variable T is not much larger than 1 for photon energies in the interesting region, for instance $T = 2 - 7$ for $\hbar\omega = 3 - 10$ GeV with $l_2 = 30$ μm and 2 μm Au targets. For targets with l_1 =10 μm and 20 μm the requirement on b is barely fulfilled. In any case, the calculated interference maxima of Baier and Katkov agree with the above quoted rule.

In [97] a similar setup is treated theoretically, although with emphasis on the low energy photons and the similarity between transition radiation from a structured target and undulator radiation.

Thus, as a continuation of the investigations of formation lengths, we wish to 'force' the electron to emit high energy photons by passing it through a foil which is in a sense too thin for the emission of many low energy photons, i.e. the formation length is longer than the foil thickness [82]. This can be done by a 'sandwich foil' technique where for example about 50 foils of a few micron thick gold are interspersed by Low Density PolyEtylene (LDPE) which has a large radiation length and thus resembles air. By this technique we can achieve a target which is thick enough to yield a high signal-to-background in H4, yet each sub-target is thin enough to suppress photons below a limit of several GeV. Initial studies of such structured targets [23] show the need for more thorough investigations, e.g. to address the question of the

[2)] Using the definition of Q as a function of n as defined in [98] yields a value of b that is a factor Z too small. We have used the definition of n from [86].

contribution from multiple scattering dominated transition radiation or the resonance peak arising from interference between radiation amplitudes from different segments of the target.

The study is relevant in several contexts, e.g. heavy ion physics, linear collider technology, coherent bremsstrahlung and transition radiation. Furthermore, direct relevance to the emission of quasi-monochromatic x-rays in this configuration has been studied theoretically [97] and may be investigated experimentally. The dependence of the emission on the coherence from different periods makes the phenomenon somewhat similar to the emission of radiation in an undulator. An analogous phenomenon is expected in QCD for the emission of soft gluons by a penetrating quark where the finite size of the nucleon may suppress the emission [88].

Taken to the extreme of energies as high as 4 TeV, a realistic sandwich target consisting of 7 micron thick sub-targets will suppress by a factor 2 the radiation below 2 TeV yielding a potential source of photons of very high energy with a reduced disturbance from low energy photons. Interferences from radiation amplitudes from subsequent foils in the stack can be studied in a scheme reminiscent of coherent bremsstrahlung, only with much larger interaction spacing [95, 98]. Last, transition radiation dominated by multiple scattering can be studied. In this regime, a 200 GeV electron may emit transition radiation in the few-GeV region, way above the 'classical' transition radiation characterized by $\gamma\hbar\omega_p$, about 3 MeV in e.g. Au with plasma frequency ω_p =80 eV/$\hbar$.

8.2 Experimental details

The proposed structure of the experimental setup for the investigation of structured targets is shown in figure 23. Its main components are 3 drift chambers, (DCs) for the definition of the entry- and exit-angles and positions on the target. Downstream the MBPL where the primary e^+/e^- are deflected, a He-tank is positioned to reduce the conversion probability of the photons. Finally, the photons are intercepted by a downstream calorimeter, consisting of either lead glass, lead tungstate or BGO crystals. The spent lepton is absorbed in a dump constructed from iron and lead blocks.

8.3 Requested beam time

The focus of this experiment is the emission of low energy photons. Since the Bethe-Heitler cross section falls off with increasing photon energy roughly as $1/\hbar\omega$, the majority of electrons emit photons of low energy and essentially all electrons accepted by the primary trigger ($\mathrm{Sc1}\cdot\mathrm{Sc2}\cdot\overline{\mathrm{Sc3}}$) are good events. Aiming for 25 bins per decade in energy, each with a 2% error bar this means 62500 events per decade in energy or about 1e6 events in total per target. Accepting 2000 events per burst, using a pessimistic down-time of 50% of the accelerator-chain and counting 4 bursts a minute, each target takes about 4 hours to complete a satisfactory statistics.

With 6 targets and a long no-target run, taking change-over time and calibration verification inbetween runs into account, this experiment is estimated to take 2 days.

We estimate the risk of failure of this sub-project to be very limited. There are no tight mechanical constraints, no alignment procedures as the targets are amorphous, and the setup consists of detectors that from previous runs are known to be reliable and predictable.

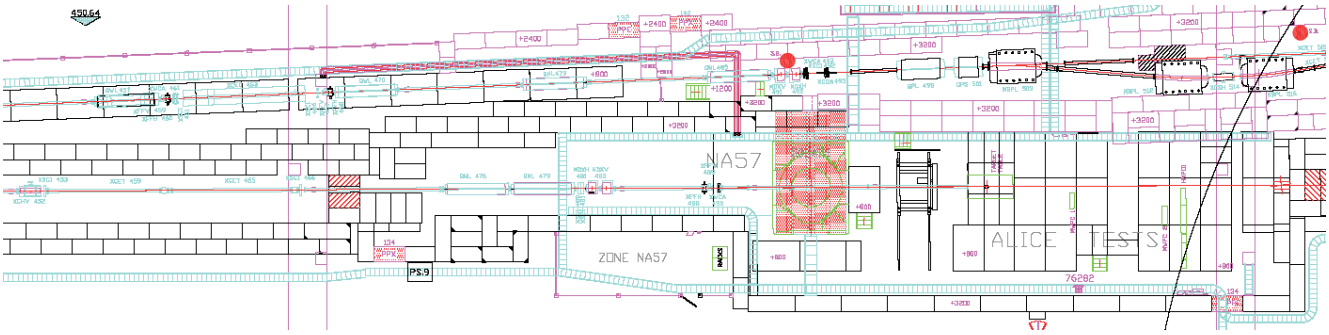

Figure 16: *A drawing of the H4 PPE124 and PPE134 zones in which the equipment is to be installed. See text for details.*

9 Equipment details

In this section, the components in common for most of the proposed measurements are described. All components are to be installed in the H4 PPE124 and PPE134 zone of the SPS, see figure 16.

9.1 Drift chambers

As position sensitive detectors, we plan to use the drift chambers previously used by e.g. NA43. These detectors are reliable, stable and relatively easy to operate and provide a position resolution of about 100 μm (σ), with a maximum tolerable intensity of about 200k electrons per burst. Positioned e.g. 10 metres apart, two of these detectors provide angular resolution of about 15 μrad (σ), comparable to the planar channeling critical angle of 100 GeV electrons ($\psi_p \propto 1/\sqrt{p}$). Furthermore, for targets that are of small dimensions in the transverse plane, the drift chambers enable a relatively clean target selection in the off-line analysis. Each drift chamber contributes about 0.1%X_0 to the background radiation, from emission during the passage of the aluminized windows.

9.2 Scintillators

For the triggering and selection of valid events, a number of scintillator counters are to be installed, typically three for the primary trigger. Of these, at least one is a veto-counter with a hole of approximate transverse dimension to cover the available target. This is particularly important for the targets of small transverse dimensions. The rate limit for the scintillators is approximately a factor 10 above that of the drift chambers and is not expected to be a limiting factor. The thickness of the scintillators not used as vetos is chosen to be 1 mm as a compromise between light-yield, i.e. efficiency, and influence on photon background through radiative loss of the primary electron beam (and radiation energy loss straggling that results in a small broadening of the photon energy distribution). The thickness of veto-counters is 1 cm.

9.3 Calorimeters

Depending on the photon energies of primary interest, we plan to use a number of different photon calorimeters. For high energy photons ($\gtrsim$ 1 GeV) lead glass blocks of appr. 25X_0 or lead tungstate of appr. 20X_0 are planned to be used. For lower energies, 10 MeV$\lesssim \hbar\omega \lesssim$ 1 GeV, BGO crystals of appr. 20X_0 are more suitable and finally, for $\lesssim$ 10 MeV photons, NaI or $LaCl_3$(Ce) crystals are to be used.

9.4 Goniometer

For the alignment of crystalline targets, the goniometer previously used by e.g. NA43 is to be installed. This goniometer consists of two stages, denoted as 'tilt' and 'turn', i.e. rotations around the horizontal axis perpendicular to the beam and the vertical axis, respectively. If needed, an 'azimuth' stage, rotation around the beam axis, is available and can be installed. Each goniometer stage (Microcontrole BGM80PPV6 and URM80PPV6) has a stepsize of $1/1000^\circ \simeq 17$ μrad, which can be further sub-divided into microsteps of $1/10000^\circ \simeq 2$ μrad. The goniometers have recently been renovated and verified for proper operation.

Alignment of crystals is done through remote control of the goniometer stages, at each step registering the radiation intensity. Upon passage (in angle space) of low-index crystallographic planes or

axes, the penetrating particle has an enhanced probability for radiation emission and the resulting radiation peaks are plotted in a stereogram, allowing verification of the crystal orientation and identification of the indices of the planes and the axis. A complete alignment of a crystal with 150 GeV electrons oriented close to an axis is known from experience to take up to about 24 hours, typically a factor 2 less, even with a laser-prealigned crystal in the beam line. The reason for this is the pre-alignment accuracy which can typically be as good as a few mrad (a tenth of a degree). With a step-size of the order one critical Lindhard angle $\simeq 10$ μrad per burst, this amounts to about 200 bursts or one hour of beam per scan of which 5-6 are required for a proper identification in the stereogram. For crystals to be aligned in a planar orientation, this procedure is significantly shorter as only one good scan is required.

9.5 Pair spectrometer

As figure 5 shows, there is good agreement between the shape of the experimental spectrum from the data of NA43 and that of the simulated spectrum. The geometrically imposed cut-offs convoluted with the resolution in both spectra, i.e. the energy thresholds in figure 5 and the differential thresholds in figure 17, show almost perfect agreement between simulation and data. In this connection it is worth noting that events with e.g. 3 particles detected in one or more of the chambers (which can be the result of the deflected primary electron not being fully contained in the dump for instance) are not simulated nor is the cross-talk between DC cells. This type of events may contribute to some extent to the difference between simulated and real data. Also the absolute value of the resolution of a drift chamber affects sensitively the high energy end of the simulated spectrum of photon energies and is thus another source of the slight disagreement there.

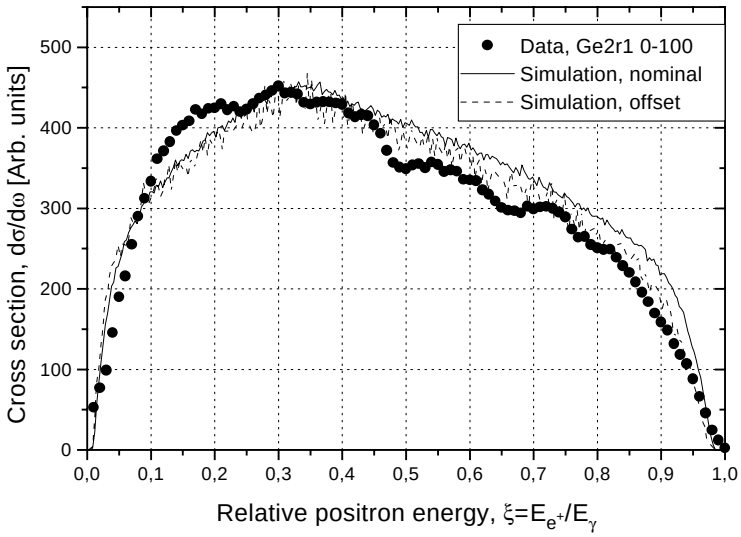

Figure 17: *Results of the Monte Carlo simulation compared with data for radiation from 0.82 mm Ge in random plus a 2 mm thick Cu foil. Relative positron energy reconstructed by use of the pair spectrometer. The filled dots are experimental points, the full-drawn curve is the simulation for the photon beam center incident on the drift chamber field wire and the dashed curve includes the measured offset with respect to the field wire.*

The shape of the energy- and differential spectra, figures 5 and 17, are far from resembling the Bethe-Heitler spectra - this is due to the geometrical constraints on the photon energy imposed by DC5. In a plot of the reconstructed photon energy, E_γ, vs. the relative positron energy, ξ_+, see figure 18, the limits are set by the minimal accepted positron energy, $E_{\mathrm{e}^+}^{\min}$, and the minimal accepted electron energy, $E_{\mathrm{e}^-}^{\min}$, as

$$E_\gamma \geq \frac{E_{\mathrm{e}^+}^{\min}}{\xi_+} \text{ and } E_\gamma \geq \frac{E_{\mathrm{e}^-}^{\min}}{1-\xi_+} \tag{27}$$

The figures 5 and 17 correspond to projections of figure 18 onto the x and y-axis. The minimal

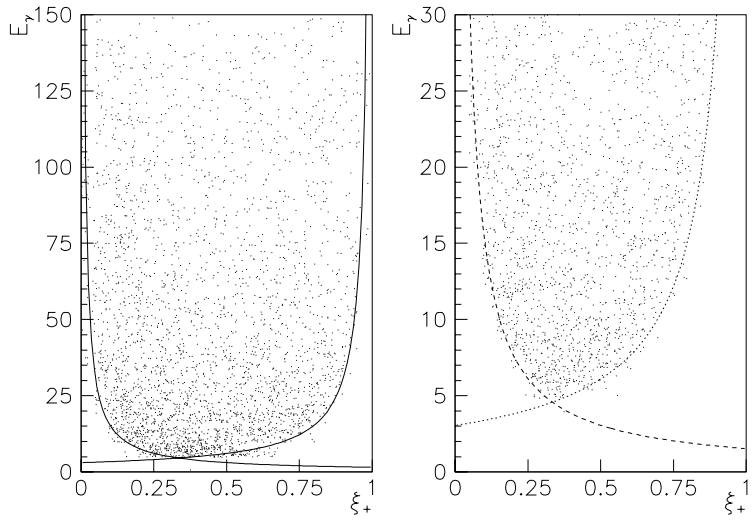

Figure 18: *The reconstructed photon energy, E_γ, vs. the relative positron energy, ξ_+, showing the limits set by the geometry from data (dots) and from eq. (27) (lines). The two graphs display the same data with different scaling of the photon energy.*

accepted energies, in this case $E_{\mathrm{e}^-}^{\min} = 3.05$ GeV and $E_{\mathrm{e}^+}^{\min} = 1.53$ GeV for the nominal beam, are inversely proportional to the transverse distance from the impact of the photon beam (the reconstructed vertex on the conversion foil) to the edge of the drift chamber, d_{edge}. This means that if the chamber is asymmetrically positioned (to avoid left-right ambiguity on the sensing anode-wire), the differential spectrum becomes asymmetric with a peak at d_{edge}/D where D is the width of the chamber. In the case shown here, $d_{\mathrm{edge}}/D \simeq 0.33$ in good agreement with data. The overall scaling of accepted momenta is according to

$$p[\mathrm{GeV/c}] = \frac{299.8 \cdot Bl[\mathrm{Tm}] \cdot L_0[\mathrm{m}]}{\Delta x[\mathrm{mm}]} \tag{28}$$

where $Bl[\mathrm{Tm}]$ is the integrated field of the magnetic dipole in Tm, $L_0[\mathrm{m}]$ is the distance in m from the center of the dipole to the position sensitive detector which measures a transverse deflection $\Delta x[\mathrm{mm}]$ in mm.

9.6 Data, read-out electronics and analysis

The signals from all detectors, subject to the trigger conditions, are registered on a CAMAC unit connected to a PC. The accepted event rate is about 2000 good events per burst. Analysis of the data is done on-line by a fast custom-made program 'Dumle' and off-line analysis is performed by converting the data-formats into n-tuples and analyzing using PAW.

9.7 Timescale and running priorities

In table 2 we summarize the sub-experiments, in terms of requested beam and beam time as well as scientific potential and assessed risk.

9.8 Requests to CERN

Full advantage of the similarity with the setup by NA43 is taken. We have renovated and tested essentially all detectors, drift chambers, scintillator counters, solid state detectors, electromagnetic calorimeters etc. No additional detectors apart from standard beam line equipment (FISCs,TRIGs) are expected to be needed.

For the tagging of photons and the separation of the spent electron from the photons, we request to have an MBPL installed, as close downstream to Goliath in H4 as possible. This position of an MBPL

Activity	Request	Risk	Potential	Beam
Setting up, cal.	5 days	-	-	10-300 GeV e, e^+
Trident	7 days	Modest	Basic QED	150-250 GeV e
Cryst. undul.	≥ 5 days	High	New 'rad. device'	$\leq$10 GeV e^+
Sandwich	2 days	Low	New resonances	150-250 GeV e
Few tens GeV	3 days	Average	Pairprod. LPM	50-80 GeV e
Spin-flip	7 days	Modest	Basic QED	10-300 GeV e^+

Table 2: *A short summary of the proposed experiments. The list is in order of decreasing priority.*

has been used during earlier testbeam activities, e.g. CHUDAKOV in 2004. Furthermore, we request to have an MDX dipole installed 10 metres downstream the MBPL. This was previously done for NA43 in 1997 in H2 and at that time this proved largely sufficient for the magnetic spectrometer.

We request a parallel beam starting at or upstream QNL 444 (QNL 476 and 479 off) of 10-300 GeV electrons/positrons derived from $\geq 2 \cdot 10^{12}$ protons on target (POT) on T2.

Some of us are already CERN users and we have the office space needed to run the experiment. As a counting room, we need access to e.g. barrack HNA343 and we need to use the gas zone previously used by ALICE as a test zone, located outside HNA148.

9.9 Manpower and economy

As essentially all the equipment is existing, there are no large costs to be covered. Our budget is roughly 100 kCHF per year for new investments, repair and developments. The main part of this budget has been obtained from the EU sixth framework programme — NEST-PECU — for the investigation of radiation effects in crystals, in particular the crystalline undulator. Besides this, the sixth framework programme funding has provided money for a strengthening of the scientific staff involved in these projects. The main emphasis in the investments for development is on the calorimeter and pair spectrometer, in order to increase the lower threshold and acceptance, respectively. We thus have the manpower and economy to improve the setup of NA43 substantially in order to address new and exciting possibilities in strong field QED.

The institute of each active participant during the experiments at CERN pays for travel, accomodation and daily expenses such as local transport. Concerning manpower, all members present at CERN will participate in covering shifts at the experiment. Moreover, the equipment does not require large manpower to be run - it is mainly controlled from two PCs, four NIM crates and a CAMAC unit, so experience shows that two persons on shift at a time is sufficient.

10 Concluding remarks

The equipment is existing, the beam is as used in NA43, i.e. 10-300 GeV electrons derived from $\geq 2 \cdot 10^{12}$ POT, and we request from CERN to give access to the beam in H4 with 1 MBPL and 1 MDX magnets installed in the zone 134. To fully benefit from the similarity of the setup with that of NA43 and the desire to go to high energy (nominally 300 GeV) it is necessary to use the H4 beam. The possibility of going to high energies (above 200 GeV) with an essentially parallel beam is essential to some of the proposed measurements. Therefore, CERN is the only place these experiments can be performed.

The presented scheme relies solely on QED processes. The comparatively high cross sections for these processes - even for higher order contributions - mean that datataking time in each case is rather limited, of the order a few days, depending on the target.

We estimate the setup and calibration time to be 5 days, so we expect that all of the mea$E_{e^+}, E_{e^-} >$ 1 GeVsurements can be performed within a total period of 2×3 weeks, e.g. in 2007 and 2008, with a setup closely analogous to that of NA43 (see above). We propose to do the 'crystalline undulator' and 'trident' experiments in the first year, to be able to return to these subjects in the following year if they fulfill our expectations. For example in the case of the 'crystalline undulator', a careful study of the behaviour with beam energy and divergence as well as crystal properties like oscillation wavelength and amplitude is desirable, given that the phenomenon as such is established.

The proposed measurements will supplement and strengthen the conclusions reached by NA43 and since the setup is very similar to that of NA43 we benefit from having run most of the equipment several times before.

References

[1] E. Uggerhøj (spokesman, NA43), CERN/SPSC 90-31-SPSC/P234; K. Kirsebom *et al.*, CERN-SPSLC-96-5; SPSLC-M-572 (1996)

[2] K. Kirsebom *et al.*, Nucl. Instrum. Methods B **174**, 274 (2001)

[3] K. Kirsebom *et al.*, Nucl. Instrum. Methods B **135**, 143 (1998)

[4] A. Baurichter *et al.*, Nucl. Phys. B (Proc. Suppl.) **44**, 79 (1995)

[5] A. Baurichter *et al.*, Phys. Rev. Lett. **79**, 3415 (2001)(and most likely also the AIR) is only applicable

[6] K. Kirsebom *et al.*, Phys. Rev. Lett. **87**, 054801 (2001

[7] V.N. Baier and V.M. Katkov, Phys. Rep. **409**, 261 (2005)

[8] V.N. Baier and V.M. Katkov, Phys. Lett. A **346**, 359 (2005)

[9] V.N. Baier, V.M. Katkov and V.M. Strakhovenko, *Electromagnetic Processes at High Energies in Oriented Single Crystals*, World Scientific 1998.

[10] Yu.V. Kononets, Europhys. Lett. **71**, 517 (2005)

[11] M.Kh. Khokonov and H. Nitta., Phys. Rev. Lett. **89**, 094801 (2002)

[12] U.I. Uggerhøj, Rev. Mod. Phys. **77**, 1131 (2005)

[13] A.H. Sørensen, Proc. NATO ASI **255**, 91, Plenum, 1991, reprinted in Nucl. Instr. Meth. B **119**, 1 (1996)

[14] R. Moore *et al.*, Nucl. Instrum. Methods B **119**, 149 (1996)

[15] N. Doble, L. Gatignon and P. Grafström, Nucl. Instrum. Methods B **119**, 181 (1996)

[16] C. Biino *et al.*, Nucl. Instr. Meth. B **194**, 417 (2002)

[17] H.D. Hansen *et al.*, Phys. Rev. Lett. **91**, 014801 (2003)

[18] H.D. Hansen *et al.*, Phys. Rev. D **69**, 032001 (2004)

[19] U.I. Uggerhøj, Mod. Phys. Lett. B **18**, 309 (2004)

[20] U.I. Uggerhøj *et al.*, Phys. Lett. B **619**, 240 (2005)

[21] E. Uggerhøj and U.I. Uggerhøj, Nucl. Instr. Meth. B **234**, 31 (2005)

[22] U.I. Uggerhøj *et al.*, Phys. Rev. C **72**, 057901 (2005)

[23] U.I. Uggerhøj *et al.*, Phys. Rev. D **72**, 112001 (2005)

[24] V.B. Berestetskii, E.M. Lifshitz and L.P. Pitaevskii, *Relativistic Quantum Theory*, Pergamon Press, New York, 1971.

[25] J. Lindhard, K. Dan. Vidensk. Selsk. Mat. Fys. Medd. **34**, no. 14, 1-64

[26] A.H. Sørensen, in *Relativistic channeling*, NATO ASI vol. 165, edited by R.A. Carrigan, Jr. and J.A. Ellison (Plenum Press, New York), p. 331-337.

[27] R.C. Duncan, *astro-ph/0002442* (2000)

[28] A.I. Ibrahim, J.H. Swank and W. Parke, Astrophys. Journ. **584**, L17-L21 (2003)

[29] R. Yamazaki, K. Ioka, F. Takahara and N. Shibazaki, *astro-ph/0502320* (2005)

[30] W. Greiner, B. Müller and J. Rafelski - *Quantum Electrodynamics of Strong Fields*, Springer, Berlin 1985

[31] D.L. Burke *et al.*, Phys. Rev. Lett. **79**, 1626-1629 (1997).

[32] C. Bamber *et al.*, Phys. Rev. D **60**, 092004 (1999).

[33] P. Chen and V.I. Telnov, Phys. Rev. Lett. **63**, 1796-1799 (1989).

[34] A.Kh. Khokonov, Khokonov, M.Kh. and R.M. Keshev, Pis'ma Zh. Tekh. Fiz. **24**, 20-27 [Sov. Tech. Phys. Lett. **24**, 797-799 (1998)]

[35] A. Kh. Khokonov *et al.*, Technical Physics **47**, 1413 (2002); A. Korol, A.V. Solov'yov and W. Greiner, J. Phys.G: Nucl. Part. Phys. **28** , 627 (2002)

[36] S.V. Bulanov, T. Esirkepov and T. Tajima, Phys. Rev. Lett. **91**, 085001 (2003).

[37] P. Chen and K. Yokoya, Phys. Rev. Lett. **61**, 1101-1104 (1988).

[38] R. Blankenbecler and S.D. Drell, Phys. Rev. Lett. **61**, 2324-2327 (1988).

[39] A.A. Watson, Nucl. Phys. B (Proc. Suppl.) **60**, 171 (1998)

[40] I. Pomeranchuk, Journ. Phys. **2**, 65 (1940)

[41] B. McBreen and C.J. Lambert, Phys. Rev. D **24**, 2536 (1981)

[42] T. Stanev and H.P. Vankov, Phys. Rev. D **55**, 1365 (1998)

[43] A.V. Plyasheshnikov and F.A. Aharonian, J. Phys. G **28**, 267 (2002)
[44] K. Shinozaki *et al.*, Astrophys. Journ. **571**, L117 (2002)
[45] T. Stanev, Nucl. Phys. B (Proc. Suppl.) **60**, 181 (1998)
[46] U.I. Uggerhøj, Nucl. Phys. B (Proc. Suppl.) **122**, 357 (2003)
[47] H. Nitta, T. Kudo and H. Minowa, Am. J. Phys. **67**, 966 (1999)
[48] P. Krekora, Q. Su and R. Grobe, Phys. Rev. Lett. **92**, 040406 (2004)
[49] J.C. Kimball and N. Cue, Phys. Rep. **125**, 69 (1985)
[50] T. Erber, Rev. Mod. Phys. **38**, 626 (1966)
[51] A.V. Korol, A.V. Solov'yov and W. Greiner, Int. Journ. Mod. Phys. E **8**, 49 (1999); W. Krause, A.V. Korol, A.V. Solov'yov and W. Greiner, J. Phys.G: Nucl. Part. Phys. **26**, L87 (2000); A.V. Korol, A.V. Solov'yov and W. Greiner, J. Phys.G: Nucl. Part. Phys. **27**, 95 (2001)
[52] M.B.H. Breese, Nucl. Instr. Meth. B **132** , 540 (1997)
[53] A. Nylandsted Larsen, private communications, 1999
[54] A.V. Solov'yov, A. Schäfer and W. Greiner, Phys. Rev. E **53**, 1129 (1996)
[55] M.L. Ter-Mikaelian - High-Energy Electromagnetic Processes in Condensed Media, Wiley Interscience, 1972
[56] J. Bak *et al.*, Nucl. Phys. B **254** , 491 (1985)
J. Bak *et al.*, Nucl. Phys. B **302**, 525 (1988)
[57] A. Baurichter *et al.*, Proc. Int. Conf. on Atomic Coll. in Solids, Odense 1999, subm. to Nucl. Instr. Meth. B
[58] J.A. Ellison, S.T. Picraux, W.R. Allen and W.K. Chu, Phys. Rev. B **37**, 7290 (1988)
[59] V.N. Baier, V.M. Katkov and V.M. Strakhovenko, Nucl. Instr. Meth. B **35**, 21 (1988)
[60] A.M. Taratin and S.A. Vorobiev, Nucl. Instr. Meth. B **31**, 551 (1988)
A.M. Taratin and S.A. Vorobiev, Nucl. Instr. Meth. B **42**, 41 (1989)
[61] S.T. Picraux, L.R. Dawson, G. Osbourn and W.K. Chu, Appl Phys. Lett. **43**, 930 (1983)
W.K. Chu, C.K. Pan and C.-A. Chang, Phys. Rev. B. **28** , 4033 (1983)
[62] A.V. Korol, A.V. Solov'yov and W. Greiner, J. Phys.G: Nucl. Part. Phys. **24**, L45 (1998)
[63] U. Mikkelsen and E. Uggerhøj, Nucl. Instr. Meth B **160**, 435 (2000); R.O. Avakian *et al.*, in Electron-Photon Interaction in Dense Media, ed. H. Wiedemann (Kluwer, 2002)
[64] S. Bellucci *et al.*, Phys. Rev. Lett. **90**, 034801 (2003)
[65] S. Bellucci *et al.*, Phys. Rev. ST Acc. Beams. **7**, 023501 (2004)
[66] R.O. Avakian *et al.*, Nucl. Instr. Meth B **173**, 112 (2001)
[67] A.V. Korol, A.V. Solov'yov and W. Greiner, Int. J. Mod. Phys. E **13**, 867 (2004)
[68] A.V. Korol, A.V. Solov'yov and W. Greiner, Proc. Int. Workshop "Channeling 2004", physics/0412101 (2004)
[69] A.V. Solov'yov, A. Schäfer and C. Hofmann, Phys. Rev. E **47**, 2860 (1993)
[70] A.V. Solov'yov and A. Schäfer, Phys. Rev. E **48**, 1404 (1993)
[71] R. Blankenbecler and S.D. Drell, Phys. Rev. D **36**, 277 (1987)
[72] S. Eidelman et al, Phys. Lett. B 592, 1 (2004)
[73] V.N. Baier, V.M. Katkov and V.M. Strakhovenko, Nucl. Instr. Meth. A **250**, 514 (1986)
[74] P.L. Anthony *et al.*, Phys. Rev. Lett. **75**, 1949 (1995)
[75] P.L. Anthony *et al.*, Phys. Rev. D **56**, 1373 (1997)
[76] N.F. Shul'ga and S.P. Fomin, JETP Lett. **63**, 873 (1996)
[77] F.F. Ternovskii, JETP **12**, 123 (1961)
[78] N.F. Shul'ga and S.P. Fomin, JETP **27**, 117 (1978)
[79] N.F. Shul'ga and S.P. Fomin, Phys. Lett. A **114**, 148 (1986)
[80] N.F. Shul'ga and S.P. Fomin, Nucl. Instr. Meth. B **145**, 73 (1998)
[81] N.F. Shul'ga and S.P. Fomin, JETP **86**, 32 (1998)
[82] N.F. Shul'ga and S.P. Fomin, Nucl. Instr. Meth. B **145**, 73 (1998)
[83] S. Klein, Rev. Mod. Phys. **71**, 1501 (1999)
[84] R. Blankenbecler and S.D. Drell, Phys. Rev. D **53**, 6265 (1996)
[85] B.G. Zakharov, JETP Lett. **64**, 781 (1996)
[86] V.N. Baier and V.M. Katkov, Phys. Rev. D **57**, 3146 (1998)

[87] B.G. Zakharov, Phys. Atom. Nucl. **61**, 838 (1998)
[88] B.Z. Kopeliovich, A. Schäfer and A.V. Tarasov, Phys. Rev. C **59**, 1609 (1999)
[89] B.G. Zakharov, JE
[90] V.M. Biryukov, V.I. Kotov, Y.A. Chesnokov, Physics-Uspekhi **37**, 937 (1994)
TP Lett. **73**, 49 (2001)
[91] B.G. Zakharov, Nucl. Phys. B (proc. suppl.) **146**, 151 (2005)
[92] E. Uggerhøj and U.I. Uggerhøj, Nucl. Instr. Meth. B **234**, 31 (2005)
[93] J.D. Jackson - Classical Electrodynamics, John Wiley, 1975
[94] V.E. Pafomov, Sov. Phys. JETP **20**, 353 (1965)
[95] R. Blankenbecler, Phys. Rev. D **55**, 190 (1997)
[96] R. Blankenbecler, Phys. Rev. D **55**, 2441 (1997)
[97] V.N. Baier and V.M. Katkov, Nucl. Instr. Meth. A **439**, 189 (2000)
[98] V.N. Baier and V.M. Katkov, Phys. Rev. D **60**, 076001 (1999)

11 Schematic drawings of proposed setups

On each of the following pages, the setup for the proposed experiments is shown e.g. to display more clearly the similarities between the setups as well as the differences.

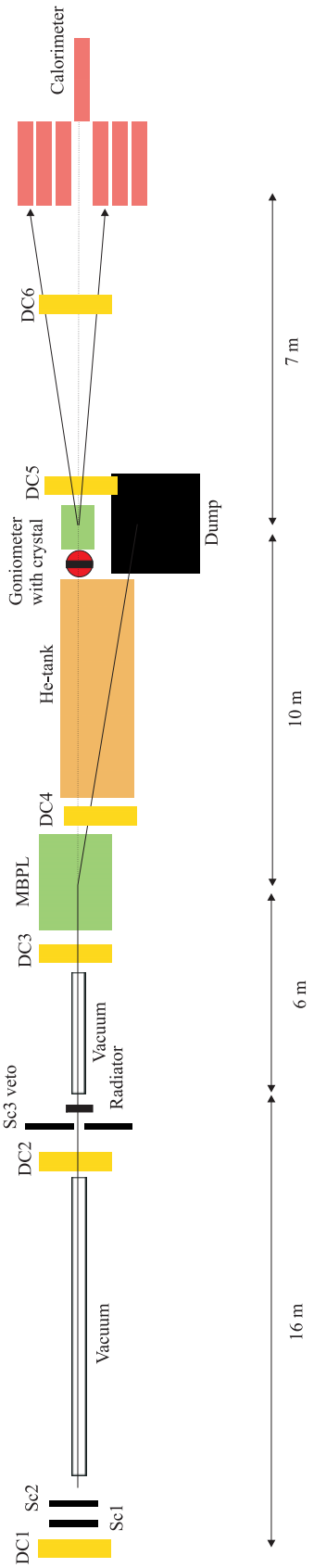

Figure 19: *A schematic drawing of the setup proposed for the investigation of trident production. See section 4.2 for details.*

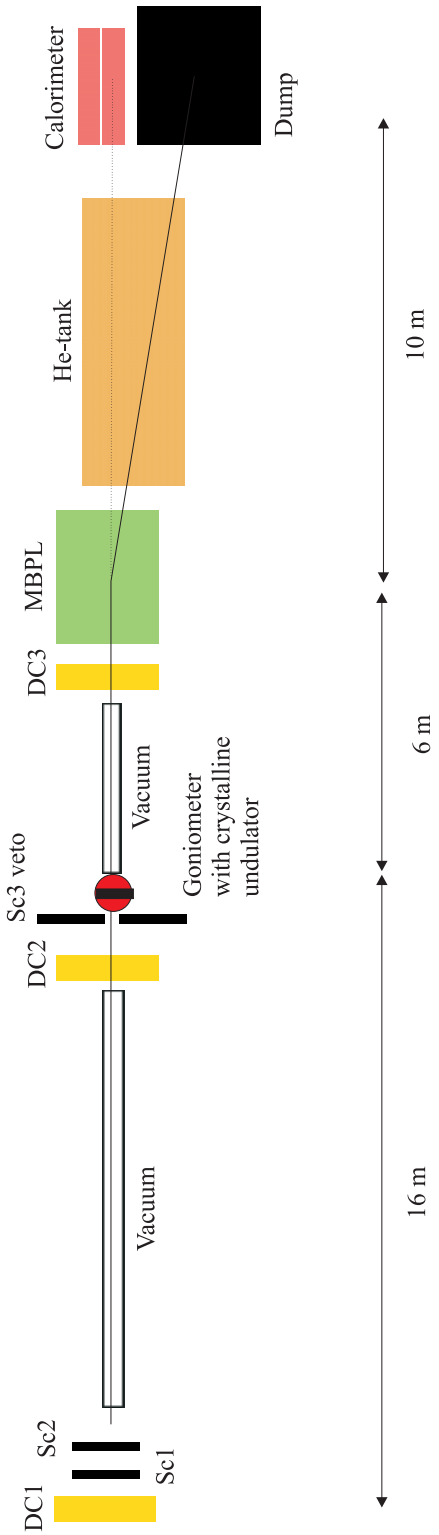

Figure 20: *A schematic drawing of the setup proposed for the investigation of crystalline undulators. See section 5.2 for details.*

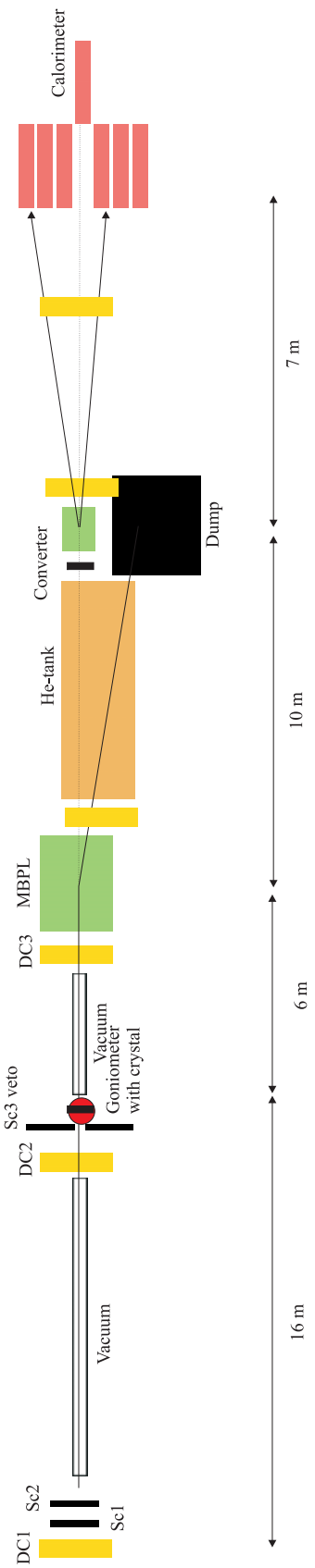

Figure 21: *A schematic drawing of the setup proposed for the investigation of the contribution from spin-flip transitions. See section 6.2 for details.*

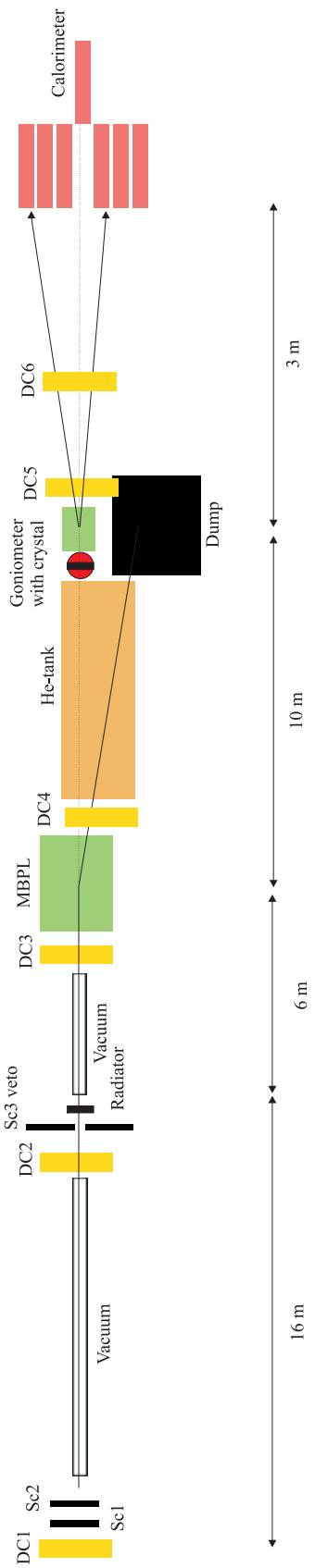

Figure 22: *A schematic drawing of the setup proposed for the investigation of the contribution from the LPM effect for pair production in the few tens GeV range. See section 7.2 for details.*

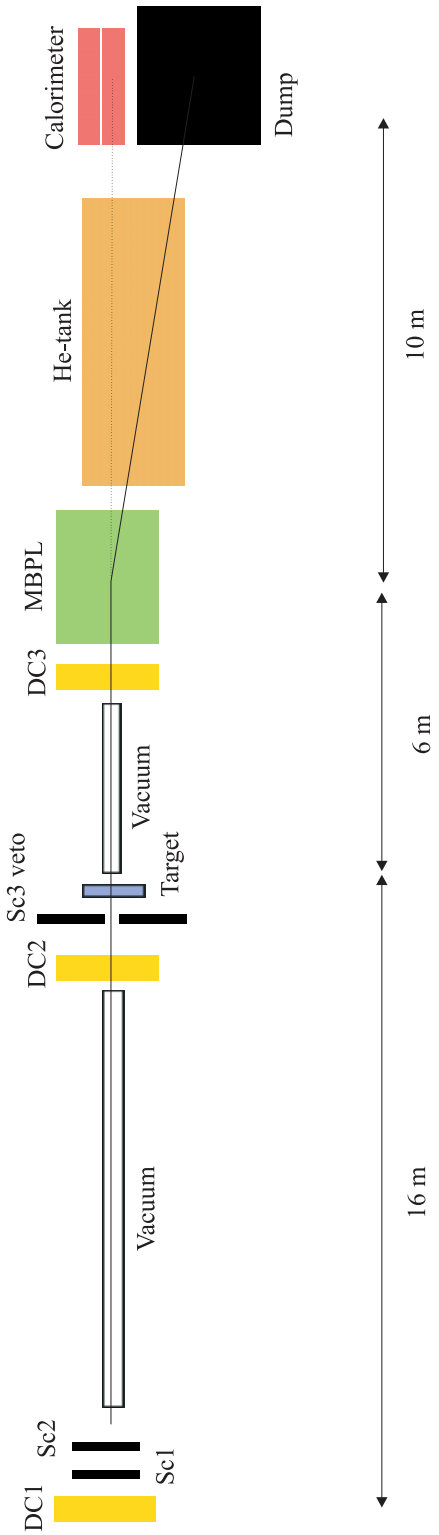

Figure 23: *A schematic drawing of the setup proposed for the investigation of structured targets. See section 8.2 for details.*